JOURNAL OF COMPUTATIONAL PHYSICS 103, 90–115 (1992)

An Efficient Surface-Integral Algorithm Applied to Unsteady Gravity Waves

J. W. DOLD

School of Mathematics, University of Bristol, Bristol BS8 1TW, United Kingdom

Received September 19, 1990; revised June 29, 1991

A computationally fast method for calculating the unsteady motion of a surface on a two-dimensional fluid is described. Cauchy's integral theorem is used iteratively to solve Laplace's equation for successive time derivatives of the surface motion and time-stepping is performed using truncated Taylor series. This allows fairly large time-steps to be made for a given accuracy while the required number of spatial points is minimised by using high order differencing formulae. This reduces the overall number of required calculations. The numerical implementation of the method is found to be accurate and efficient. A fairly thorough examination of this implementation is carried out, revealing that high accuracies are often achievable using surprisingly few numerical surface points. Extensive calculations are also performed using modest computing resources. Some numerical instabilities are identified, although these would not usually be significant in practical calculations. A model analysis reveals that two of these instabilities can be eliminated by using suitable methods of time-stepping. Should the third "steep-wave instability" become significant, it is shown that it can be completely controlled by using high-order smoothing techniques, at little cost to accuracy. Using a routine to ensure asymptotic conservation of energy, this is confirmed by time-stepping a very steep (but stable) wave over thousands of wave-periods.

1. INTRODUCTION

Since all of the interior properties of a body of fluid undergoing inviscid, incompressible irrotational motion are fully determined by properties at its boundary, it is possible to reduce the calculation of the motion of such a fluid to the evaluation of the motion of its surface alone. In a numerical scheme, the entire motion can thus be modelled using only a point discretisation of the surface.

Such an approach was first suggested by Svendsen in 1971 as a means of calculating the motion of two-dimensional gravity waves on water [1]. Since then the idea has been implemented using a variety of boundary-integral or conformal mapping techniques, by Longuet-Higgins and Cokelet [2], Vinje and Brevig [3], Baker, Meiron, and Orszag [4], Roberts [5], Fornberg [6] and (based on his original formulation) by Svendsen and co-workers [7]. Although this paper presents yet another numerical method, the approach is aimed specifically at producing a computationally fast and efficient numerical scheme in order to be able to study problems of increased complexity.

In numerically representing complicated surface motions, ranging from the breaking of waves to the evolution of instabilities in a train of travelling waves, it typically becomes necessary to use a large number of surface points. If running times tend to increase too rapidly with the number of points, then this can destroy any apparent advantage in being able to treat the whole fluid only in terms of its moving surface. The penalty is particularly severe for algorithms that require matrix inversion or factorisation techniques—yielding running times per time step that increase like N^3 (the cube of the number of surface points). By using iterative techniques, the penalty can be reduced to running times per time-step that increase in proportion to N^2. While being less severe, this still has the effect that increased numbers of surface points become increasingly expensive to calculate. The use of a conformal mapping technique [6] can lead to running times per time-step that vary like $N \log N$. However, this method is severely limited in its ability to resolve steep wave surfaces (as are found in breaking waves), requiring disproportionately many surface points to achieve a given accuracy.

It is therefore vital to ensure computational efficiency if it is to be possible accurately to describe wave processes for which large numbers of surface points may be required. The most direct way of achieving this is to employ the lowest number of points that can *adequately* describe a fluid surface. In this paper, a further improvement is introduced by showing that higher time-derivatives of the motion can be calculated directly using exactly the same technique that is used to determine the velocity of the surface at each time-step. This yields significantly more information about the motion for relatively little extra computation. In turn, this allows larger time-steps to be performed for a given accuracy so that the overall number of calculations can be reduced. The method presented here combines these two ideas into producing a practical numerical algorithm, the properties of which are examined in the following pages.

In Appendix A, the formulae are derived that make it

0021-9991/92 $5.00

possible to calculate not only the velocity but also acceleration, the rate of change of acceleration and, in principle, any successive time derivative of the surface motion, given only the shape of and velocity potential on the surface at some instant in time. The usefulness of this extra information and its practical limitations are discussed. In fact these formulae can be used in conjunction with any one of the boundary integral or conformal mapping methods that are currently available for evaluating the gradient of a potential function at a surface from its values given along the surface.

A brief outline is made of some of these methods for solving Laplace's equation at a boundary. Of these we select the use of Cauchy's integral theorem as potentially one of the simplest and most accurate to implement, one that has not previously been reported to lead to numerical instabilities in following the two-dimensional motion of a fluid surface, and one that can be solved efficiently by iteration. Using a "point-label" parameter and insisting that computational points must be "smoothly" distributed along the surface, high order central differencing formulae are used to approximate the surface and to estimate the values of spatial derivatives. With these formulae, fewer points can be used to maintain a given accuracy than would be possible using lower-order differencing formulae or (say) linear surface elements—as in [3]. The numerical implementation (including the accommodation of the singularity of the integral kernels) is straightforward.

In order to put these ideas to the test, a program was written for following the evolution of periodic wave surfaces. In this, tenth order (11-point) polynomial estimates are used to solve the surface boundary value problem—in the form of Cauchy's integral theorem—for the first three time-derivatives of the surface motion. Using (say) l_B previously calculated values of the third time-derivative, polynomial-fitted backward differencing is used to enhance the accuracy of time-stepping in the form of a Taylor series truncated to the order of $l_B + 3$. The order of backward differencing that is used for this, l_B, can be set to any value between two and five. Variable time-steps are chosen in order to set the estimated errors due to time-stepping, for quadratic backward differencing ($l_B = 2$), to a specified value.

A number of sample calculations are presented in order to illustrate the accuracy and computational speed of the algorithm, including its economical requirement on the number of surface points. Some specifically unsteady calculations are also presented in order to illustrate the scheme's ability to cope with small and large scales of wave-breaking as well as very long-time (non-breaking) evolutions of an unsteady wave-surface. These are performed accurately and remarkably quickly, requiring relatively few numerical points to describe the surface. As far as they go, these simulations also display no obvious signs of numerical instability and no deliberate steps were taken to prevent any such an instability. On a useful practical level, unsteady nonlinear processes such as the formation of fairly sharp wave crests and fluid jets in (for example) breaking waves or wave impacts, or the interactions of longer and shorter waves, are reproduced well by the numerical scheme.

A problem of great interest, that has been reported to arise with most of the existing numerical schemes for following the motion of surface gravity waves, is the presence of a "sawtooth" numerical instability. This was first encountered by Longuet-Higgins and Cokelet [2], who used smoothing techniques to control it. An oscillation of successive points along the surface is found to grow from one time step to the next. It has been conjectured (Moore [8]) that the instability arises through an artificial numerically induced resonance interaction between the actual wave motion being modelled and short waves whose wavelength is about twice the particle separation on the surface. Finite numerical schemes, which are necessarily based on discrete approximations of continuous functions, may be unable correctly to model the dispersion relation for such short wavelengths. If the frequency of the motion of this shortest resolvable wavelength is artificially as low as the frequency of the basic wave, then a numerically induced resonance becomes highly likely.

The algorithm, as implemented in this paper, produces a numerical dispersion relation for small-amplitude waves in which frequency increases monotonically as wavelength decreases down to, and including, the wave described by only two surface points (a "sawtooth" wave). As a result, resonance is highly unlikely, and indeed the resolution and calculation of short wavelengths of about two or three grid points often seems to contribute significantly to the accuracy and efficiency of the scheme.

However, despite appearing to be numerically stable under many circumstances, a number of examinations reveal that the algorithm is, in fact, subject to at least three distinct forms of possible numerical instability. When using excessively large time-steps, one encounters a *strong instability* that appears and grows dramatically in very few steps. This is not surprising since explicit time-stepping is used. A simple stability analysis for the time-stepping of a model periodic problem reveals the manner in which the size of time-step leads to this instability when increased above a certain threshold value. Results accord well with some calculated numerical growth and decay rates. This strong instability is easily eliminated by appropriately restricting the size of time-step.

The model stability analysis also predicts a fairly rich picture for the ranges of numerical stability or instability for different orders of backward differencing. In particular, it predicts another form of *weak instability* that will normally always be present (however small the time-step) when quadratic or cubic backward differencing is used, i.e., $l_B = 2$ or 3. Selected calculations show that this instability tends to be most significant when calculating small amplitude waves

over hundreds of wave-periods. Again, this weak instability is easily eliminated by using quartic or quintic backward differencing—the model analysis indicates that quintic differencing produces a wider window of stability (as well as being asymptotically more accurate at small time-steps).

A third form of numerical instability is beyond the scope of this simple model analysis to predict. Investigating a number of test-cases, a *steep-wave instability* is revealed. In following steady surface waves, the rate of growth of this instability is found to correlate surprisingly well with properties found at the peak of the wave, most particularly with the curvature of the wave-surface at that point. As such, it is still encountered for small amplitude waves, albeit over a very much prolonged time-scale. It is conjectured that this steep-wave instability is (at least partly) due to major errors in numerically simulating the group velocity of very short wave-modes, having wavelengths of about two to three grid points. Although the use of spectral methods for calculating derivatives, rather than high-order finite differencing, should improve the description of these modes [5] and so (possibly) remove the instability, these are not examined in this paper.

More worryingly, the test investigations indicate that the steep-wave instability is always found to appear (for any size of time-step or order of backward differencing) in calculations that are able to continue over a sufficiently long period. This would present a major difficulty in attempting to calculate the asymptotically long-time evolutions of wave surfaces if the instability could not be prevented. Fortunately, this can be done by using smoothing techniques. Although their use is less satisfactory than having a numerically stable scheme, some useful variations of the smoothing formulae derived by Longuet-Higgins and Cokelet [2] are discussed in Appendices B and C. While succeeding in removing any very short wavelength components in the surface data, higher-order smoothing formulae are shown to be much more selective and so to cause less loss of accuracy. A number of useful formulae (for variable-step backward differencing, 11-point polynomial-fitting and derivative calculation, as well as routines for ensuring asymptotic conservation of energy and mean-level), are also presented in Appendices B and C.

The role of these numerical instabilities should not be exaggerated. By appropriately choosing the order of backward differencing, by suitably limiting the maximum size of time-step and, if necessary, using a degree of smoothing, the scheme seems to be free of all numerically induced instability. Rather, it is important to understand the manner in which instabilities may arise in order to know how they may be removed or avoided. It is then possible to have greater confidence in the overall accuracy of the numerical method and to be sure that any calculated surface motion reflects a real property of the mathematical model rather than some purely numerically induced phenomenon.

Most importantly, the scheme that is described and analysed in this paper is able quickly to perform highly accurate numerical calculations of gravity-waves. Equivalently, this means that a wide range of increasingly complicated and interesting wave phenomena can be studied even with relatively modest computing resources [9–14].

2. DESCRIPTION OF THE FLUID MOTION

2.1. Basic Model

For inviscid, irrotational,[1] and incompressible flow, a velocity potential $\phi(\mathbf{r}, t)$ exists and satisfies Laplace's equation,

$$\nabla^2\phi = 0. \tag{2.1}$$

If the fluid is contained by a fixed impermeable bottom or lower boundary $\mathscr{B}$ then the condition that no fluid penetrates this bottom requires that the normal gradient ϕ_n of ϕ must be zero:

$$\phi_n(\mathbf{r}, t) \equiv 0 \qquad \text{for} \quad \mathbf{r} \in \mathscr{B}. \tag{2.2}$$

In most of this paper only a horizontal bottom at $y = -h$ is considered, for which the bottom boundary condition becomes,

$$\phi_y(x, -h, t) \equiv 0. \tag{2.3}$$

However, it is worth noting that this is not such a special case as it may appear since the methods applicable to a boundary at $y = -h$ can be extended to any situation where the boundary $\mathscr{B}$ can be transformed into a flat horizontal boundary under a conformal mapping [14] (cf. Section 3).

The upper boundary of the fluid region can be considered to consist of a time-dependent surface $\mathbf{r} = \mathbf{R}(\xi, t)$, on which it is convenient to define the parametric variable ξ to represent a particle-following (Lagrangean) coordinate. Sufficient boundary conditions with which to solve Laplace's equation for ϕ anywhere within the fluid region are then provided by specifying the values of ϕ on the surface—that is by defining $\phi(\mathbf{R}(\xi, t), t) = \Phi(\xi, t)$. In particular, the normal gradient ϕ_n of ϕ at the surface can be found, at least in principle. Since the tangential gradient ϕ_s (s denotes the arclength) is obtainable by direct differentiation of Φ and $\mathbf{R}$ with respect to ξ as follows

$$\phi_s = \Phi_\xi / |\mathbf{R}_\xi|, \tag{2.4}$$

[1] A straightforward extension of the method to a flow with uniform vorticity appears in Ref. [15].

the velocity of the fluid at the surface can be determined using

$$\mathbf{u} = \nabla\phi = \phi_s \hat{\mathbf{s}} + \phi_n \hat{\mathbf{n}} \tag{2.5}$$

where $\hat{\mathbf{s}}$ and $\hat{\mathbf{n}}$ are tangential and normal unit vectors, respectively.

It is possible to use this information for integrating forwards in time both the surface profile $\mathbf{R}(\xi, t)$ and the surface values of the potential $\Phi(\xi, t)$; a kinematic condition, that fluid particles move with their own velocity,

$$\frac{D\mathbf{r}}{Dt} = \mathbf{u} \tag{2.6}$$

and a "dynamic" condition for an inviscid fluid, given by Bernoulli's equation,

$$\frac{D\phi}{Dt} = \frac{1}{2}\mathbf{u}^2 - P/\rho - gy \tag{2.7}$$

provide the necessary information for doing this. In the latter equation, the fluid density is ρ and g represents the acceleration due to gravity in the direction of decreasing y.

The way in which the pressure P is specified on the surface must depend on the nature of the particular situation being modelled. The simplest description is to define it as a constant (say zero) representing the case in which surface tension is negligible and where any upper fluid, such as the atmosphere, is considered light enough to cause no significant variation in hydrostatic or dynamic pressure. Surface tension can be included by defining P as

$$P = P_0 - \sigma\kappa, \tag{2.8}$$

where P_0 is the pressure on the exterior side of the surface, σ is the coefficient of surface tension, and κ is the curvature of the surface given by

$$\kappa\hat{\mathbf{n}} = \mathbf{R}_{ss} = (\mathbf{R}_\xi/|\mathbf{R}_\xi|)_\xi/|\mathbf{R}_\xi|$$

or

$$\kappa = (X_\xi Y_{\xi\xi} - Y_\xi X_{\xi\xi})/(X_\xi^2 + Y_\xi^2)^{3/2}, \tag{2.9}$$

where $\mathbf{R} = (X(\xi, t), Y(\xi, t))$. Appropriate choices of P (or P_0) can be made to approximate the effects of wind over a wave surface, or to generate the motion of a "pressure-forced" wave [2]. It is also possible to calculate P from the motion of another fluid above the surface [4].

Once the surface pressure P is obtainable at any time t, and the velocity $\mathbf{u}$ can be obtained by solving Laplace's equation (2.1) with ϕ specified on the surface, it becomes possible to integrate equations (2.6) and (2.7) with respect to time—at least on the surface. In principle, given their values at any initial moment, this provides a full description of the evolution of the surface profile $\mathbf{R}$ and surface potential Φ. By discretising time and the fluid surface, these formulae can be implemented numerically to provide a computational algorithm for following the development of surface gravity-waves [1–7].

2.2. Use of Higher Time Derivatives

It is useful to note that a procedure for solving Laplace's equation (2.1) for the gradient ϕ_n—given the bottom boundary condition (2.2) and the values of ϕ on the surface—can also be used to obtain the gradient of any harmonic potential function in exactly the same way. In particular, by differentiating (2.5), (2.1), and (2.2), it is easily seen that successive Eulerian time derivatives of ϕ, namely ϕ_t, ϕ_{tt}, etc., satisfy both Laplace's equation and the same bottom boundary condition as ϕ. Moreover, these derivatives are the potential functions for the corresponding Eulerian time derivatives of velocity:

$$\begin{aligned} &\mathbf{u}_t = \nabla\phi_t, \quad \nabla^2\phi_t = 0, \quad (\phi_t)_n = 0 \quad \text{for } \mathbf{r} \in \mathscr{B}, \\ &\mathbf{u}_{tt} = \nabla\phi_{tt}, \quad \nabla^2\phi_{tt} = 0, \quad (\phi_{tt})_n = 0 \quad \text{for } \mathbf{r} \in \mathscr{B}, \end{aligned} \tag{2.10}$$

etc.

In Appendix A, the detailed formulae are derived with which this property can be exploited to determine any number of Lagrangean time-derivatives of the surface profile and potential. In essence, given $\mathbf{R}$ and ϕ on the surface at a time t and a means of solving for $\nabla\phi$, which thus gives the velocity $\mathbf{u}$, the value of ϕ_t on the surface can be found and used to obtain $\nabla\phi_t$ in the same way. From this, the acceleration $D\mathbf{u}/Dt$ can be calculated as well as the surface values of ϕ_{tt}. Similarly, by obtaining $\nabla\phi_{tt}$ the next time-derivative can be calculated and, in principle, the procedure can be continued indefinitely. It is thus possible successively to determine up to any order of time derivative of the velocity from a knowledge only of the surface profile and velocity potential at the surface. Using these derivatives, the time-dependence of $\mathbf{R}$ and ϕ can be expressed in terms of Taylor series expansions.

However, in a numerical solution of the motion of a surface which is approximated by a finite number of discrete moving points, it becomes impractical to continue the calculation of higher derivatives indefinitely. The first difficulty arises in programming the appropriate forms of the equations derived in Appendix A. It is clearly seen that the calculations become progressively more complicated at each higher order and that there is no simple way of automating the procedure. The second and most basic difficulty arises in maintaining accuracy. The order of nonlinearity and the order of spatial derivative involved

in the calculations increase with each order of time derivative calculated. Ultimately, the ability to make accurate numerical estimates, particularly of high orders of spatial derivatives, is limited by the adequacy of the discretisation of the surface. With steep surface phenomena, such as wave breaking, the problem of calculating spatial derivatives is exacerbated by the tendency for dramatic changes in properties to take place over relatively small portions of the surface. Nonlinearity exaggerates such changes in the higher orders, which thus tend to lose accuracy more readily for steep waves than for weakly nonlinear waves.

Nevertheless, the calculation of a limited number of higher order derivatives can be performed accurately for little added computational effort. With this information, it is possible to carry out the numerical time-integration of equations (2.6) and (2.7) more accurately for a given size of time-step using truncated Taylor series; if n is the order of the first derivative neglected in setting up the Taylor series for $\mathbf{R}$ and Φ then the error for a time-step size of δt is of the order of $\delta t^n/n!$. This provides a significant improvement over more straightforward algorithms that use only first-derivatives.

On the other hand, for a given accuracy, larger time-step sizes can be tolerated, potentially providing a substantial improvement in running time. Setting up matrices with which to solve Laplace's equation on a given surface $\mathbf{R}$ tends to be a lengthier task than the use of these matrices to obtain any particular solution. As a result, the advantage obtained by being able to use a larger time step for a given final accuracy is disproportionately high; running time is reduced by requiring the task of setting up the matrices to be performed much less frequently.

3. METHODS FOR SOLVING LAPLACE'S EQUATION

The ability to follow the wave-surface motion depends entirely on being able to solve Laplace's equation (2.1). A number of practical numerical methods for doing this have been developed, with varying degrees of efficiency and accuracy [1–6]. An outline of some of these methods follows:

The use of Green's identity on the velocity potential ϕ,

$$\phi = \oint (\phi G_n - G\phi_n)\, ds, \tag{3.1}$$

together with the Green's function for Laplace's equation, $G(\mathbf{r}, \mathbf{r}') = \ln|\mathbf{r}' - \mathbf{r}|$, provides one such approach, as implemented by Longuet-Higgins and Cokelet [2] in 1976. Discretisation of this equation requires special treatment of the logarithmic singularity and leads to a system that is not easily solved using iterative means. By using matrix inversion or diagonal factorisation the resulting penalty, of running times that increase as the cube of the number of points, is especially severe for large values of N.

The use of Green's identity on the stream function ψ,

$$\psi = \oint (\psi G_n - G\psi_n)\, ds, \tag{3.2}$$

which, after using the Cauchy–Riemann relations,

$$\phi_n = -\psi_s \qquad \text{and} \qquad \phi_s = \psi_n, \tag{3.3}$$

becomes

$$\psi = \oint (\psi G_n - G\phi_s)\, ds, \tag{3.4}$$

provides another possible approach [1]. The values of ϕ_s on the surface are "known," being obtainable by differentiating Φ along the surface as in (2.4), so that only ψ is unknown. Having solved for ψ, the arclength derivative ψ_s gives ϕ_n from the appropriate Cauchy–Riemann relation (3.3). Representing a Fredholm integral equation of the second kind in ψ, the resulting equations are more suitable for solution by iteration with running times that increase only as the square of the number of points.

In a slightly different formulation of the problem, the surface can be considered to form a vortex sheet with potential flow on either side of it [4, 5]. Although the integral equation arising from this method can be solved iteratively, solving for higher time derivatives is not as straightforward since pressure plays a different role.

A conformal mapping technique which maps a wave profile onto a flat surface was developed by Fornberg [6]. In the mapped plane Laplace's equation is still satisfied, and for deep water its solution becomes trivial in such a simple domain. The time taken to establish and carry out such a conformal mapping thus determines the running time, and by Fornberg's method this increases only in proportion to $N \ln N$. However, it appears that such methods may have difficulty in coping accurately with steep wave phenomena such as the jets formed during wave breaking.

Singularities such as dipoles, vortices or sources placed outside the body of the fluid can be used to approximate the complex potential within the fluid. This approach was implemented by McIver and Peregrine [16], who used a least-squares technique applied at discrete surface points to estimate the strength and position of external singularities. While obtaining remarkable accuracy in calculating flow fields using surprisingly few singularities, a least-squares approach in determining positions, strengths, and orientations of singularities requires the repeated solution of sets of linear equations until a good fit is reached. Each solution takes of the order of the cube of the number of unknown quantities. Thus, a few singularities can be determined quite quickly while many will take considerably longer. For strongly nonlinear or complicated surfaces involving

(say) many distinct waves, this would prove severely disadvantageous.

Cauchy's integral theorem can be applied to the complex potential $\zeta(r) = \phi + i\psi$ which, for Laplace's equation (2.1) to be satisfied, is an analytic function of the complex position, $r = x + iy$. Vinje and Brevig [3] made use of this property by discretising the profile $r = R(\xi, t) = X + iY$ (in complex notation) into linear elements and using the following principal value form of Cauchy's integral theorem at each vertex,

$$\zeta(R) = \frac{1}{i\theta} \int \frac{\zeta(R')}{R' - R}\, dR' \tag{3.5}$$

where θ is the internal angle between linear elements at the vertex at a point R, and where the integration is performed in an anticlockwise sense over a single closed contour. The resulting set of equations is suitable for solution by iteration. In contrast to the logarithmic singularity of the Green's function, the simple reciprocal singularity of the Cauchy integral kernel is relatively easily taken into account in numerical approximations.

4. USE OF CAUCHY'S INTEGRAL THEOREM

Because of its relative simplicity, Cauchy's integral theorem was selected as the basis for testing and developing a new numerical scheme with which to follow the evolution of a complex wave-surface using directly calculated higher time derivatives. However, we use a different formulation of the integral equation from that used by Vinje and Brevig [3], and consider the surface to consist of a smooth continuous profile, approximated (to high order) by a set of discrete points, rather than comprising linear elements. It should be remembered that the use of Cauchy's integral theorem is only one choice among several possibilities, and that alternative means of solving potential functions [17, 18] could prove equally valuable.

4.1. Formulation

For any harmonic function ϕ, the complex potential gradient defined as $q(r) = \phi_x - i\phi_y$ is an analytic function of $r = x + iy$. In this, as in Section 3.6, the convention that r is the complex equivalent of the position vector $\mathbf{r} = (x, y)$ has been introduced. Similarly, $R(\xi, t)$ is taken to be the complex equivalent of the surface profile vector, $\mathbf{R} = (X, Y)$. It may be noted that the arclength derivative $R_s = R_\xi / |R_\xi|$ is the complex unit tangent and that iR_s is the unit normal in the 90° anticlockwise rotated direction. Thus, with ϕ_s and ϕ_n respectively denoting the tangential and normal gradients of ϕ measured in these directions, q can also be defined such that

$$q^* = \phi_x + i\phi_y = R_s(\phi_s + i\phi_n) \tag{4.1}$$

where * denotes the complex conjugate. Applying Cauchy's integral theorem (3.5) to $q(r)$ on a *smooth* closed contour (so that θ is exactly π at all points) now gives

$$\phi_s - i\phi_n = \frac{R_s}{i\pi} \int \frac{\phi'_s - i\phi'_n}{R' - R}\, ds'. \tag{4.2}$$

Rearranging this, ϕ_n is found to satisfy the integral equation

$$\pi\phi_n = \int \mathrm{Im}\left(\frac{R_s}{R' - R}\right) \phi'_n\, ds' + \int \mathrm{Re}\left(\frac{R_s}{R' - R}\right) \phi'_s\, ds', \tag{4.3}$$

where the arclength s' is a scalar variable which is taken (in this equation) to increase in an *anticlockwise* sense around one entire closed contour. The primed variables, R', ϕ'_s and ϕ'_n, are evaluated at points on the surface corresponding to s'.

The horizontal-bottom condition (2.3) can be taken into account by assuming that the fluid extends continuously below $y = -h$ to a reflection of the surface in the bottom, as shown in Fig. 1a. The motion of this reflected surface must exactly mirror the real surface so that the reflection condition

$$q(R^* - 2ih) = q^*(R) \tag{4.4}$$

will hold. The Cauchy formula (4.3) can now be applied to the contour formed by combining the surface with its reflection, leading to the integral equation,

$$\pi\phi_n = \int \mathrm{Im}\left(\frac{R_s}{R' - R} + \frac{R_s}{R'^* - R - 2ih}\right) \phi'_n\, ds' + \int \mathrm{Re}\left(\frac{R_s}{R' - R} - \frac{R_s}{R'^* - R - 2ih}\right) \phi'_s\, ds', \tag{4.5}$$

in which s' is taken to increase from *right to left* along the surface only. In cases where the contributions to the integrals at large negative and positive values of x can be estimated analytically, this equation can be used as the basis for a numerical scheme to solve interatively for ϕ_n. This would be the case, for example, in studying solitary waves or hydraulic jumps [11, 14].

For the purpose of exploring the method, however, it is sufficient and perhaps most illustrative to focus attention on situations in which the surface is periodic in x. No generality is lost in taking time and space dimensions to be suitably scaled to make this period exactly 2π. The infinite fluid surface is then transformed into a finite closed contour by the conformal mapping for which

$$\Omega(\xi, t) = \exp(-iR(\xi, t)), \tag{4.6}$$

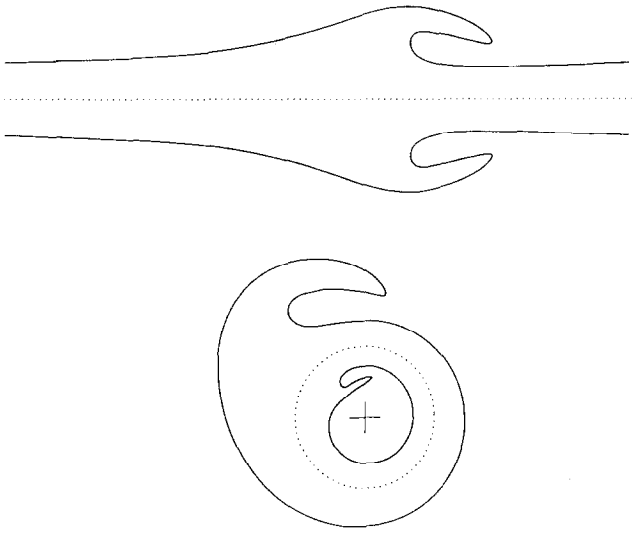

FIG. 1. Example of a periodic surface and reflection transformed into closed contours. The impermeable flat bottom is shown dotted.

as shown in Fig. 1b. The Cauchy formula (4.3) can now be applied to the combination of this contour and the transformation of the reflected surface, at which condition (4.4) is applied. Expressing the resulting integral equation in terms of the parameter ξ rather than s it becomes

$$\pi\phi_v = \int \mathrm{Im}\left(\frac{\Omega_\xi}{\Omega-\Omega'} + \frac{\Omega_\xi}{\Omega - H/\Omega'^*}\right)\phi'_v\, d\xi' + \int \mathrm{Im}\left(\frac{\Omega_\xi}{\Omega-\Omega'} - \frac{\Omega_\xi}{\Omega - H/\Omega'^*}\right)\phi'_\xi\, d\xi', \quad (4.7)$$

where $H = \exp(-2h)$, ϕ_ξ is the derivative of ϕ with respect to ξ along the surface, and where ϕ_v is the normal gradient of ϕ in the physical **r**-plane, scaled by $|R_\xi|$. The reversed sign of the integral kernels in this equation, compared to (4.3) and (4.5), is adopted because we now choose (purely for convenience) to integrate in a *clockwise* sense, as ξ' increases from *left to right* on the surface. Provided this equation can be solved for ϕ_v, the complex potential gradient of ϕ in the physical plane is then given by

$$\phi_x + i\phi_y = i\frac{\Omega^*}{\Omega^*_\xi}(\phi_\xi + i\phi_v) = (\phi_\xi + i\phi_v)/R^*_\xi. \quad (4.8)$$

It can be noted that the term arising from the bottom condition in the integral kernels of equation (4.7) does not vanish as $H \to 0$ (that is $h \to \infty$). This seems surprising since it must be possible to omit the term completely for a "bottomless fluid"—which may be considered to be almost synonymous with a "fluid of infinite depth" (one for which contribution to the integrals. It can therefore by subtracted from this term, changing it to

$$\frac{H\Omega_\xi/\Omega'^*}{\Omega(\Omega - H/\Omega'^*)}, \quad (4.9)$$

which does vanish as $h \to \infty$. Besides making the equations continuous with their form for a "bottomless fluid," this makes a considerable difference to the diagonal dominance of the matrices representing the integral kernels and hence to the iterative behaviour of the final numerical scheme. The effect is so dramatic that the algorithm actually improves from being iteratively divergent, when the alteration is not made, to being convergent.

4.2. Implementation for Periodic Surface

In order to solve equation (4.7) numerically it is now convenient firmly to identify ξ as a point-label parameter, for which $\mathbf{R}(\xi, t)$, or $R(\xi, t)$, and $\Phi(\xi, t)$ are taken to be known only at *integer values* of ξ. The values inbetween are assumed to vary smoothly and continuously as functions of ξ so that reasonable estimates of R and Φ at any non-integer values of ξ can be made. Most particularly, derivatives with respect to ξ can be estimated. It is also possible to estimate integrals with respect to ξ as required in equation (4.7). Indeed, because the functions are all periodic in ξ and values are known at evenly spaced (unit-interval) values of ξ the best available quadrature formula for integration over one whole period reduces to a simple trapezium or (equivalently) step-function approximation.

By considering a Taylor series expansion for Ω' it can be seen that

$$\frac{\Omega_\xi}{\Omega-\Omega'} = \frac{1}{\xi-\xi'} + \frac{\Omega_{\xi\xi}}{2\Omega_\xi} + O(\xi'-\xi). \quad (4.10)$$

Thus only the real part of $\Omega_\xi/(\Omega-\Omega')$ is genuinely singular. The imaginary part is made continuous by replacing its value at $\xi' = \xi$ with $\mathrm{Im}(\Omega_{\xi\xi}/2\Omega_\xi)$. By subtracting $\phi_\xi/(\xi-\xi')$ from the real part in Eq. (4.7), this is also made continuous as follows,

$$\int_0^N \mathrm{Re}\left(\frac{\Omega_\xi}{\Omega-\Omega'}\right)\phi'_\xi\, d\xi' = \int_{\xi-N/2}^{\xi+N/2}\left[\mathrm{Re}\left(\frac{\Omega_\xi}{\Omega-\Omega'}\right)\phi'_\xi - \frac{\phi_\xi}{\xi-\xi'}\right]d\xi' + \phi_\xi\int_{\xi-N/2}^{\xi+N/2}\frac{d\xi'}{\xi-\xi'}, \quad (4.11)$$

where N is the number of points on the surface. The last

$$\mathrm{Re}\left(\frac{\Omega_\xi}{\Omega-\Omega'}\right)\phi'_\xi-\frac{\phi_\xi}{\xi-\xi'}$$
$$=\mathrm{Re}\left(\frac{\Omega_{\xi\xi}}{2\Omega_\xi}\right)\phi_\xi-\frac{\phi'_\xi-\phi_\xi}{\xi'-\xi}+O(\xi'-\xi)$$
$$=\mathrm{Re}\left(\frac{\Omega_{\xi\xi}}{2\Omega_\xi}\right)\phi_\xi-\phi_{\xi\xi}+O(\xi'-\xi). \qquad (4.12)$$

Using this result to replace the value at $\xi'-\xi$ the integrand becomes continuous and excellent estimates for the results of the contour integral can be obtained using a step-function approximation. Except at the point $\xi'=\xi$, the subtraction of $\phi_\xi/(\xi-\xi')$ can be seen to have no overall effect. It can thus be omitted, leading to the following quadrature representation of the integrals of equation (4.7)

$$\pi\phi_\nu(\xi)=\sum_{\xi'=1}^{N}\mathscr{A}(\xi,\xi')\,\phi_\xi(\xi')-\phi_{\xi\xi}(\xi)+\sum_{\xi'=1}^{N}\mathscr{B}(\xi,\xi')\,\phi_\nu(\xi'),$$

where

$$\mathscr{A}+i\mathscr{B}=-\left(\frac{H\Omega_\xi/\Omega'^*}{\Omega(\Omega-H/\Omega'^*)}\right)^*+\begin{cases}\dfrac{\Omega_\xi}{\Omega-\Omega'}: \xi'\neq\xi\\[2ex] \dfrac{\Omega_{\xi\xi}}{2\Omega_\xi} \quad : \xi'=\xi\end{cases} \qquad (4.13)$$

(using the modified form (4.9) of the bottom contribution).

5. NUMERICAL IMPLEMENTATION

5.1. Basic Procedure

A program was written using the formulae (4.13) to solve for potential gradients. Given a smooth periodic discretisation of the surface, the transformation (4.6) is made and the matrices of Eq. (4.13) are calculated. With Φ defined on the surface, the same matrices are used to calculate up to the third Lagrangean time-derivatives of $\mathbf{R}$ and Φ by the methods described in Appendix A and Section 3.2. Starting with relatively short time-steps, a variable-step backward differencing procedure (described in Appendix C) is applied to the previous l'_B values of the calculated third derivatives to estimate up to l'_B further time-derivatives, where the order of backward differencing l'_B is incremented at each time-step from zero (at the start) to a maximum value of $l_B\leqslant 5$ after l_B time-steps. At each step, a truncated Taylor series of order l'_B+3 is then used to march the surface values of $\mathbf{R}$ and Φ forward in time, involving a typical error (due to time-stepping) of the order of $(\delta t)^{l'_B+4}$ per time step.

Apart from an initial relatively short time-step, the size of time-step δt that is normally used for this is calculated as the geometric mean of the time-step sizes that would make the maximum contributions within the Taylor series of the third and fourth derivatives equal to a specified small "precision" parameter ε. As the wave surface develops, the size of time step is thus automatically varied more-or-less to compensate for the vigour of the motion. Also with this choice of time-step, running times, which are approximately proportional to $t/(\delta t)$, become of the order of $O(t\varepsilon^{-7/24})$, so that a reduction in the value of ε by a factor of 10 results in about a doubling of running time. Using only two orders of backward differencing, the accumulated error (due to time-stepping) over $t/(\delta t)$ time-steps becomes of the order of $O(t\varepsilon^{35/24})$; with higher orders of backward differencing, time-stepping is generally more accurate than this.

In practice, the allowable size of time step may sometimes need to be restricted below this choice. For a given point distribution at any given stage in an evolution, repeated time-steps larger than some threshold size lead to a strongly growing numerical instability that must clearly be avoided if accuracy is to be maintained. This is discussed in more detail later in Section 7. In fact, in order to demonstrate the existence and effect of this strong instability, time-steps were not restricted below this threshold value in the example calculations presented below. Briefly, the strong instability threshold is most likely to be exceeded for increased point-densities on the surface, for increased values of ε (because these tend to increase the size time-step) and for larger values of l_B (which tend to reduce the instability threshold). Naturally enough, when time-steps are limited in this way, running times no longer vary significantly with ε and the accuracy of time-stepping is typically better than predicted in the previous paragraph.

Reduced step-sizes are also, occasionally, chosen either to ensure that calculated surface data can be obtained at pre-selected times or, particularly when l'_B is increasing near the start of a calculation, to prevent time steps from increasing more rapidly than a chosen ratio (usually about 1.3).

The same parameter ε is also used to determine the appropriate stage at which iteration for the potential gradients may cease. Because each order m of derivative contributes an amount to the time-stepping that is of order $O((\delta t)^m/m!)$, it is consistent with the expected accuracy of time-stepping to calculate the normal potential gradient for derivatives of order m to an accuracy of only $m!\,\varepsilon^{(6-m)7/24}$. The solution is considered to be adequate when the maximum change over three successive iterates is significantly less than this value. The overall rate of iterative convergence is enhanced by applying Shank's transform,

$$f'_0=f_1+\frac{(f_0-f_1)(f_2-f_1)}{f_0-2f_1+f_2}, \qquad (5.1)$$

after every two iterations, where f represents any one of the surface values of ϕ_ν. This formula is based on assuming a geometric progression for the sequence of iterates f_0, f_1, and

f_2 towards (or even away from) a solution, and resets the values of ϕ_v to the limit of the progression. This is then used as the starting point for the next two iterations. The effect of this formula was found to be remarkable enough that, without including the modification (4.9) to the integral equation, accurate solutions were obtained even for otherwise diverging iterations! The total number of iterations is further reduced by using linear backward differencing to predict a good starting value for iteration from the solutions at two previous times.

As illustrated in the examples below, it is occasionally found to be either necessary or useful to use additional procedures in order to perform specific manipulations of the surface data. For example, "smoothing" of the calculated surface values may be used to inhibit the formation of significant short-wave modes (having a wavelength of the order of two or three grid points). Since, as seen later in Fig. 6, the behaviour of such short modes is calculated with an error in frequency of up to about 17%, this may be used as a means of ensuring that only those modes that are much more accurately calculated are allowed to contribute to a given numerical simulation. Smoothing formulae may also be used (if necessary) to provide some control over numerical instability [2] (see Appendix B), or as a means of ensuring that data points remain "smoothly" distributed.

A second procedure is designed to ensure that the mean surface level and energy would remain globally conserved. This is especially useful in following wave evolutions over a very long time where asymptotically meaningful results are only possible if energy is conserved. This and the procedures for smoothing are discussed in Appendix B.

Many of the calculations, including setting up the matrices (4.13) and making the transformation (4.8), involve calculating derivatives with respect to the point-label ξ. The accuracy with which this can be done, using a minimal point density, is vital to the efficient running of the numerical scheme. It is possible to use a fast Fourier transform or spectral technique for this, but the global nature of this method was felt to be undesirable in that a local inaccuracy or lack of "smoothness" about any one point would immediately affect the results at every other point. Instead it was decided to use high-order polynomial-based formulae. Estimates of the first and second derivatives using centrally based 11-point (10th order) fitted polynomials were used; the formulae for these are presented in Appendix C. The worst error arising from the use of these formulae is asymptotically very small indeed, being a relative error of the order of $|\delta \mathbf{r}/2|^{10}$, while values at more than five points distant have no effect.

5.2. Some Examples

5.2.1. *Propagation of a Steep Steady Wave*

The program was tested using highly accurate initial data for a steep deep-water periodic wave of constant waveform with amplitude $ak = 0.42$. This wave has a height that is about 95% of that of the steepest wave; it is also very close to the steady wave, of amplitude $ak \approx 0.4292$, which has maximum energy and above which steady waves become unstable to normal mode perturbations of the same wavelength as the basic wave [19]—this is described as a "superharmonic" instability by Longuet-Higgins [20]. It may be noted that the steady wave of maximum energy at $ak \approx 0.4292$ carries only about $\frac{3}{4}$% more energy than the wave of height $ak = 0.42$. The initial data were obtained using a method (described elsewhere [21]) which gives a distribution of points on the wave-surface that reproduces itself every time any one point passes through that part of the wave previously occupied by its neighbouring point. In many ways this is an optimal point distribution since, effectively, the local point-density over any section of the surface remains constant as the wave propagates.

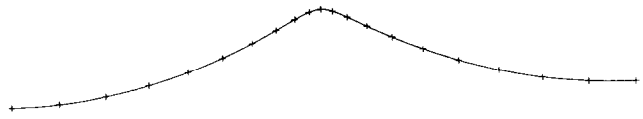

FIG. 2. Propagation of a steep steady periodic wave of amplitude $ak = 0.42$ using 20 points. The initial continuous surface is shown as well as the surface points (marked +) after five wave-periods (natural scale).

With a value of 10^{-4} for ε, taking $l_B = 2$, and using only 20 surface points, the wave was allowed to propagate for five periods. Figure 2 shows the initial wave and the points for the same wave at the end of that time. The final points coincide with the initial wave profile to well within graphical accuracy. The mean phase-speed resulting from the unsteady calculation was found to be in error by only 0.0012%, while the final values of the wave height and total energy were found to be within 0.049% and 0.009%, respectively, of their initial values. There was no sign of any numerical instability and, in calculating this example, the program used 2 $\frac{1}{2}$ min of CPU time on a SUN 3/50 desktop workstation fitted with a floating-point processor.[2] All quoted running times below were obtained on this relatively small computer.

5.2.2. *Small-Scale Breaking of a Steep Unsteady Wave*

Using the same initial surface properties for steady propagation in deep water, the steep steady wave described above was perturbed by suddenly applying a flat-bottom condition at $h = 3$. (The mean surface level in the initial data lay at $y = 0$, and it may be recalled that the wavelength is taken to be exactly 2π). As should be expected, the wave did

[2] This is approximately equivalent to the time a VAX 750 computer would require. An IBM compatible XT personal computer, fited with a mathematics coprocessor operating at 8 MHz took only 7 $\frac{1}{2}$ min to perform the same calculation.

not maintain its initial waveform but steepened on its front face until, shortly after two wave periods, a small section near the peak of the wave overturned. A detail of this portion of the wave is shown in Fig. 3. For illustration, dotted lines are placed at 120° to each other near the breaker. This corresponds to the angle of the sharp corner at the crest of the limitingly highest steady wave. Taking $l_B = 2$ and using a value of 10^{-5} for ε and 40 surface points, this example took 10 min to compute.

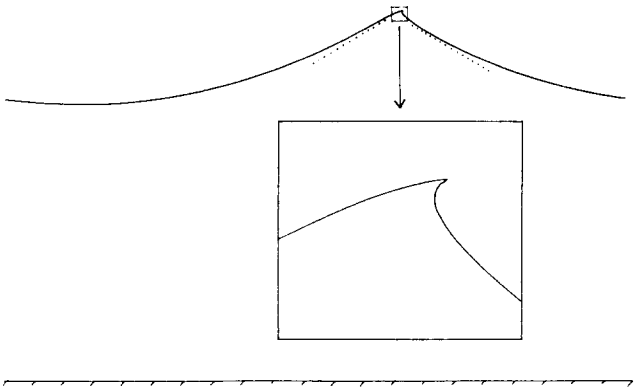

Fig. 3. Detail of a small-scale breaker formed after applying a flat-bottom at $h = -3$ to the wave in Fig. 2 (natural scale).

5.2.3. *Large-Scale Breaking of a Steep Unsteady Wave*

A much larger breaker was produced in the same way, by imposing a shallower depth of $h = \frac{1}{2}$. The peak of this wave overturns in about half of a wave-period, producing a large jet of fluid that is projected forward. Successive profiles of this big breaker are shown in Fig. 4. Using 60 surface points, $l_B = 2$ and $\varepsilon = 10^{-5}$, this test of the program took $13\frac{1}{2}$ min to run.

5.2.4. *Evolution of a Modulation*

A modulation of 10% was applied to a periodic train of eight carrier-waves of amplitude $ak = 0.09$ in deep water. At maximum growth of this modulation some waves in the group are increased to an amplitude at which they are just short of breaking [12]. It was found to be adequate to use only 8 points per wave with ε set equal to 10^{-4}—this maintains an accuracy of about 0.15% per wave-period in following a steady wave of amplitude $ak = 0.09$. The evolution was then allowed to continue for 400 wave-periods. Any drift in the total energy and mean-surface level over this long time scale was eliminated using the procedures described in Appendix B. Fifth-order backward differencing, $l_B = 5$, was used in this calculation.

Figure 5 shows an isometric view of the time-development of the surface profile, sampled every two linear wave-periods when the wave positions and wave-group are very nearly coincident—the linear speed of propagation of the

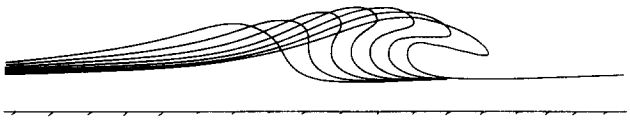

FIG. 4. Successive profiles in the formation of a large-scale breaker formed by imposing a flat-bottom at $h = \frac{1}{2}$ to the wave in Fig. 2 (natural scale).

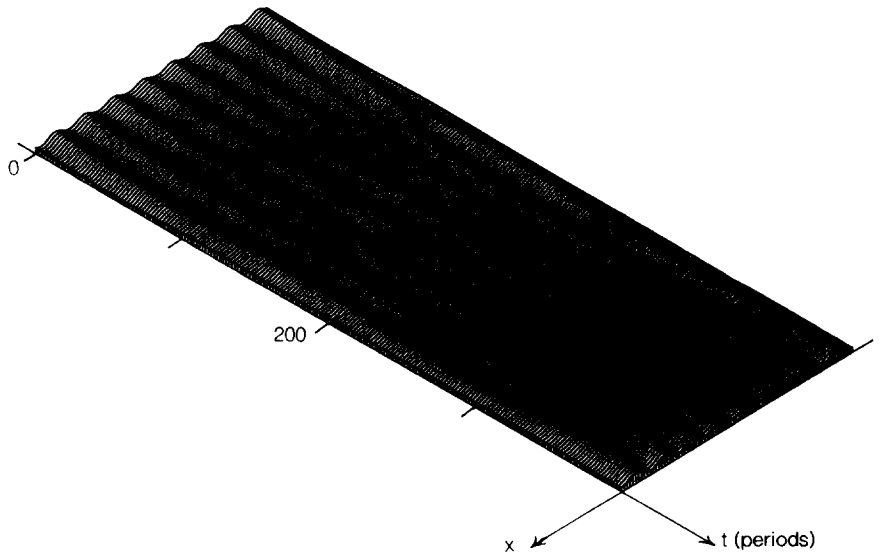

FIG. 5. Time-development of a modulated train of eight surface-waves of amplitude $ak = 0.09$ over 400 wave-periods. The surface is plotted at every second *linear* wave-period, shifted by the group velocity $c_g = c/2$.

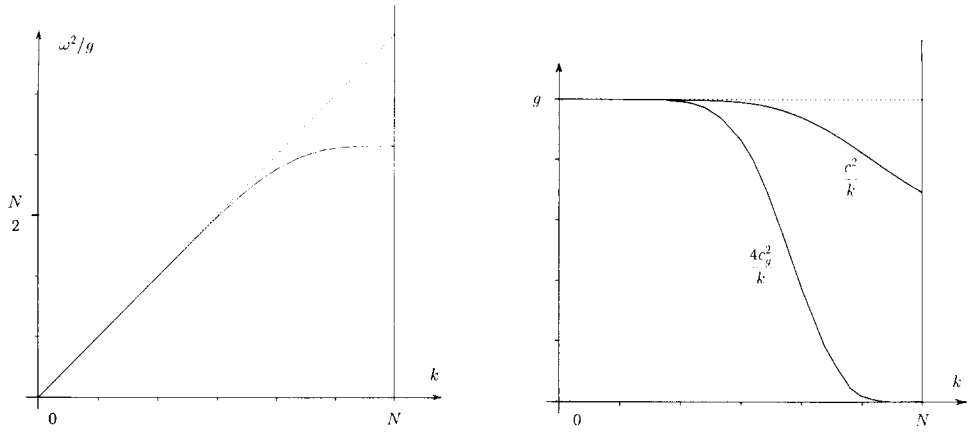

FIG. 6. (left) Numerical dispersion relation (solid line) compared with the exact relation (dotted line); (right) comparison between the numerical phase speed c, group velocity c_g, and their "exact" values (shown dotted).

wave group is about half that of the waves themselves in deep water. This extensive calculation took 12 h of CPU time to compute on the SUN 3/50 computer.[3]

6. ACCURACY AND SPEED

While also providing some illustrative examples of wave motion, the results described above give some indication of the capabilities and properties of the program. The following tests provide a more quantitative view of the properties of the algorithm, with the primary aim of investigating its accuracy, speed, and any other limitations.

6.1. Dispersion Relation

The linear dispersion relation for sinusoidal deep-water gravity-waves shows that the wave-frequency ω satisfies $\omega^2 = gk$, where k is the wave-number. Supposing that N surface points, uniformly spaced in x between 0 and 2π, are used on the surface to describe very small amplitude waves, then up to $N/2$ independent wave-numbers can be introduced and examined numerically. The wave with wavenumber $k = N/2$ is described by only two points per wave period. By numerically calculating the frequency of very small amplitude sinusoidal standing waves described by differing numbers of points per period, the numerical wave-frequency for each wavenumber between 1 and $N/2$ could be compared with the frequency predicted by the linear dispersion relation. In obtaining these results, the precision level was set to 10^{-5} multiplied by the amplitude of the waves, and very small time-steps were imposed to ensure that the resulting phase relations are, effectively, independent of any iterative convergence or time-stepping errors.

Figure 6a presents this comparison in terms of a graph of [illegible] straight line of slope g. The numerical results can be seen to underestimate the frequency by about 17% for wavenumbers of around $N/2$, by about 3% around $N/3$, and the results become extremely good as the wavenumber is reduced to below about $N/4$. At this wavenumber, only four points are being used to describe each wave and yet the frequency is accurate to better than $\frac{1}{2}$%. The variation of phase speed $c = \omega/k$ and group velocity $c_g = d\omega/dk$ (deduced from the numerical dispersion relation) are presented in Fig. 6b, along with the ideal linear-wave values of $c = 2c_g = (g/k)^{1/2}$. While the numerical phase-speed is at least qualitatively correct (although in error by up to about 17%) in the region of $k = N/2$, the group velocity erroneously decreases to zero as k approaches $N/2$. The accuracy of the numerically calculated dispersion relation can be seen to follow a similar pattern to the accuracy found for the numerical [illegible] differentiation formulae (C.8)—plotted in Fig. 12.

6.2. Dependence on Program Parameters

6.2.1. *Number of Points*

Using the same steep steady wave of amplitude $ak = 0.42$ as was used in Section 5, the program was tested over five particle or phase periods (see table caption) using different numbers of surface points. Using two orders of backward differencing, the percentage changes found in wave height, mean surface level (as a percentage of wave-height) and total energy, the error in the mean phase-speed, and the running time are all shown in Table I.

It can be seen that the program succeeds remarkably well in maintaining the basic properties of this large wave using

[3] For comparison, this calculation took 82 min of CPU time on a SUN-4 (SparcStation 1) and 51 CPU min on a Stardent computer containing four P2 processors. By using the four processors in parallel (with little vectorisation), the latter machine actually used an elapsed time of only 13 min.

TABLE I

The Effect of Point Density on Performance for a Wave of Height $ak = 0.42$, Calculated Using $\varepsilon = 10^{-5}$ and $l_B = 2$

Number of points	Percentage change over five periods in: Wave-height	Mean-level	Total energy	Phase speed	Running time (s)
8	0.46087	−0.05501	−0.44617	0.16299	93
10	−0.03252	−0.01174	−0.10861	0.04666	129
12	0.12610	−0.00296	−0.02859	0.01433	154
15	0.04562	−0.00044	−0.00381	0.00337	209
20	0.01144	−0.00002	0.00023	0.00047	327
24	0.00364	−0.00002	0.00025	0.00013	452
30	0.00073	−0.00002	0.00013	0.00003	697

Note. The change in total wave height is calculated over five particle periods while the remaining quantities are calculated over five phase periods.

as few as 10 to 15 points. Even when represented by only eight surface points, the errors per period are of the order of 0.1 % or less. The running time in these examples is found to increase in approximate proportion to $N + N^2/20$, reflecting the quadratic dependence of the iterative method of solution on the number of surface points (when calculated using a scalar processor).

6.2.2. *Precision Control Parameter, ε*

In order to investigate the effect of changes in the precision parameter ε, this same wave was observed over five wave-periods using the values of ε shown in table II. Thirty points were used in this test of the program.

The accuracy per wave period of the program in calculating the mean-surface level, total energy, and phase-speed of the wave can be seen from this to be reasonably well approximated by the predicted estimate of $\varepsilon^{35/24}$ for values of ε smaller than about 3×10^{-4}. Also, as expected, changing the precision parameter by a factor of 10 results in a change in the running time by a factor of about 2.

However, the total wave-height, which is measured from the highest extrapolated point to the lowest, does not appear to be so well conserved. This is partly an indication that the accuracy of about 0.001 % obtained for very small values of ε is as good as can be achieved using only 30 points. This view is backed up by the observation that a difference of approximately 0.0014 % is found in comparing the amplitudes of Fourier decompositions of the initial steady-wave data obtained using 30 points and 120 points. The more accurate data (based on 120 points) was used in providing initial conditions for calculating Table II, but it seems clear that 30 points remain unable to represent this data to an accuracy of better than about 0.001 %.

More fundamentally, it is found that steady calculations of this steep wave cannot be continued indefinitely. Despite the fact that such a wave should be "stable" to short-wavelength perturbations (those longer than the basic wavelength are eliminated by imposed periodicity), a growing disturbance is found to lead to a breakdown in the numerical calculations that is discussed further in the next section. In particular, the program becomes unable to continue computing the motion after the number of periods shown in the rightmost column of Table II. It can be seen that this failure appears sooner for larger values of ε (which involve larger explicit time-steps) so that the wave heights shown for ε greater than about 3×10^{-4} are noticeably affected by this unsteady transient.

6.2.3. *Order of Backward Differencing, l_B*

The effect of different orders of backward differencing on this calculation was investigated by imposing different values of l_B (between two and five) in following the wave of amplitude $ak = 0.42$ using 30 surface points and $\varepsilon = 10^{-4}$. The resulting basic properties of the wave after two wave-periods are shown in Table III.

TABLE II

Dependence of Performance on ε for a Wave of Height $ak = 0.42$, Calculated Using 30 Surface Points and $l_B = 2$

ε	Percentage change over two periods in: Wave-Height	Mean-level	Total energy	Phase speed	Running time (s)	Breakdown at period
10^{-3}	—	−1.10570	−1.17859	0.07692	92	2.0
3×10^{-4}	−0.25462	−0.00136	0.00096	0.00007	91	3.9
10^{-4}	0.00493	0.00032	0.00121	0.00002	134	6.6
3×10^{-5}	0.00160	0.00006	0.00021	0.00001	206	11.0
10^{-5}	0.00100	0.00000	0.00006	0.00001	277	15.6
3×10^{-6}	0.00087	0.00000	0.00001	0.00001	406	22.3
10^{-6}	0.00086	0.00000	0.00000	0.00001	584	30.6

Note. The percentage change in wave-height is based on two particle periods as in table I.

TABLE III

Dependence of Performance on the Order of Backward Differencing l_B for a Wave of Height $ak = 0.42$, Calculated Using 30 Surface Points and $\varepsilon = 10^{-4}$

	Percentage change over two periods in					
l_B	Wave-height	Mean-level	Total energy	Phase speed	Running time (s)	Breakdown at period
2	0.00493	0.00032	0.00121	0.00002	134	6.6
3	−0.00073	−0.00007	−0.00016	0.00000	137	6.6
4	−0.00021	0.00000	0.00010	0.00001	136	7.2
5	0.00429	0.00008	0.00033	0.00002	139	6.5

Note. As before, the percentage change in wave-height is based on two particle periods.

These calculations show that some increase in the order of backward differencing tends to produce some enhancement of accuracy, although this enhancement is lost as the order of backward differencing is increased further. The effect on running time is negligible. It is also clear that some instability is still present for all values of l_B between two and five and, because breakdown occurs at more or less the same time in each case, this instability appears to be relatively independent of the order of backward differencing, at least for large amplitude waves and small values of ε.

7. STABILITY

The numerical breakdown observed in Tables II and III shows that, at least for the control parameters l_B and ε used in these calculations, some numerical instability is present. As has already been shown in the examples calculated in Section 5, these instabilities are not necessarily a hindrance to making realistic calculations, but their presence is a cause for concern. In other similar numerical algorithms [2] (much more strongly plagued by the growth of a 'sawtooth' mode), smoothing was used to maintain stability. As described below, this is equally effective in this algorithm. However, a more detailed understanding of the nature of any numerical instability can be very valuable in revealing how it may be avoided. Moreover, understanding the nature of any underlying instability and the way in which it is being controlled allows one to have greater confidence in any calculated results.

A referee suggested that because it is not certain that the mathematical model for the wave-surface is well defined for all time, some of the difficulties may be due to the non-linearities of the model and not to the numerical method. It is indeed true, in general, that solutions can develop singularities in finite time. The known evolution of some unsteady or unstable solutions towards the formation of sharp jets or overturning breakers, which reconnect with a lower part of the surface as already calculated in Figs. 3 and 4, are cases in point. However a stable, steadily propagating wave solution [19, 20], such as that calculated in Tables II and III, should exist for all time, and so a good numerical method should at least be able to reproduce such a solution for a very long time, if not indefinitely.

In examining the stability of the algorithm, we use two approaches. The first is the examination of a range of cases. We calculate the full unsteady evolution of stable steadily propagating waves of different amplitudes with different numbers of points for different values of the parameters l_B and ε. In fact, even though there is often no apparent problem for a long time, all of these calculations are eventually found to break down and, by observing the ways in which the times to breakdown vary from case to case, one can surmise that there are three possible forms of instability.

Next, an analytical study of the linear stability of the numerical method for a flat surface reveals the cause of two of these instabilities. It also shows how a suitable choice for l_B and a restriction on the maximum allowable size of time-step can be used to remove these instabilities. The third instability still appears to be present, albeit usually very slowly growing. The root cause of this instability is not examined in this article, although it is speculated to arise from the poor description of the group velocity c_g for the shortest resolvable wavelengths, as discussed in Section 6.1. However, by way of a test case, it is shown that this instability can be completely eliminated using very selective smoothing, leading to an asymptotically stable and accurate numerical scheme.

7.1. Weak, Strong, and Steep-Wave Instabilities

7.1.1. *Steep-Wave Instability*

The instability observed in Section 6.2 also appears to arise and to behave similarly for lower amplitude waves that are not close to the "superharmonic" instability threshold [19, 20]. The main difference arising at lower amplitudes is that the time-scale over which the instability leads to breakdown is lengthened, as illustrated in Table IV. Interestingly, for each of the values of ε shown in this table, the

TABLE IV

Wave Amplitudes and Values of ε

	Amlitude, ak						
ε	0.4292	0.42	0.40	0.35	0.30	0.20	0.10
3×10^{-4}	2.2	3.9	6.2	12.2	20.3	58.0	157.3
10^{-4}	4.3	6.6	10.8	20.7	34.6	98.6	383.8
3×10^{-5}	7.4	11.0	18.7	35.1	59.4	166.2	623.9
10^{-5}	10.0	15.6	25.6	54.7	93.8	246.3	984.5
$\lvert P_n/\kappa\rvert_{\max}$	0.102	0.162	0.282	0.602	1.01	2.50	7.27

Note. Calculations are performed using 30 points and $l_B = 5$.

times to breakdown for waves of different amplitudes seem to remain in approximately the same ratio to each other. These times all increase as the wave-steepness decreases, and it is also interesting to observe that there appears to be a fairly close correlation between them and the magnitude of the radius of curvature of the wave surface at its peak (based on a wavelength of 2π), multiplied by the normal pressure gradient at that point, as presented in the final row in Table IV.

Also, broadly speaking, the times to breakdown increase by a factor between about $2\frac{1}{3}$ and 3 as ε is reduced by a factor of 10. It is worth noting for each of these calculations that, when ε is small, the wave propagates without change of form for many time-steps before an instability becomes apparent. Disturbances are then still found to grow at a relatively slow rate (per time step). Nevertheless, these disturbances eventually swamp any "real" data being calculated. Because the steepness of the wave makes a considerable difference to the time-scale over which this instability grows, it seems reasonable to identify it as a "steep-wave instability."

From the consistency of the results in Table IV, one might be led to believe that there is only this single form of

TABLE V

Numbers of Periods to Breakdown for Different Values of ε and Different Orders of Backward Differencing for a Moderately Steep Wave and for a Gentle Wave

	l_B for $ak = 0.1$ and $N = 20$				l_B for $ak = 0.3$ and $N = 40$			
ε	2	3	4	5	2	3	4	5
10^{-2}	5.95	7.47	4.31	6.09	1.77	1.61	1.60	1.30
3×10^{-3}	400	27.0	8.21	6.97	4.42	3.41	2.67	2.51
10^{-3}	614	66.5	41.2	38.5	7.88	7.55	7.53	7.40
3×10^{-4}	391	172	279	784	14.9	14.9	15.4	14.5
10^{-4}	581	597	900	951	25.8	25.6	26.8	23.6

Note. To ensure that breakdown was not due to (say) an excessive drift in total energy, procedures for conserving energy and mean level were employed during the long calculations for the wave of steepness $ak = 0.1$.

There appear to be at least two other identifiable forms of instability, as illustrated by the two wave calculations presented in Table V.

7.1.2. *Strong Instability*

It can be seen that a second rapidly growing type of numerical instability is encountered when time-steps are sufficiently large. Over only a few steps, a disturbance in the numerical data is found to appear and to grow catastrophically, quickly rendering the calculation meaningless. For the wave of steepness $ak = 0.3$ with $\varepsilon = 10^{-2}$ solutions broke down after between only 15 time-steps (for $l_B = 5$) and 20 time-steps (for $l_B = 2$). This instability has mostly been avoided in the calculations presented previously by choosing relatively small values of ε and N. However, it is clearly discernible in Table V for increased values of ε (which result in increased sizes of time-step)—one can observe that there is a fairly abrupt decrease in the time-scale over which the calculations break down. Also, unlike the results for the "steep-wave instability" of Table III, the time-scales over which the solutions break down now depend on the order of backward differencing. This "strong instability" appears at shorter time-steps (smaller values of ε) and typically grows more rapidly when l_B is larger.

7.1.3. *Weak Instability*

At smaller values of ε (say $\varepsilon = 10^{-4}$) for which the "strong instability" is avoided the two calculations in Table V break down differently. As in Table III, the time at which the calculation of the steeper wave breaks down is relatively unaffected by the order of backward differencing. Breakdown also occurs earlier than for the corresponding calculations in Table IV (indicating some reduction through increased point-density). These features all tend to indicate that the failure in these calculations is at least dominated by the same "steep-wave" instability.

By contrast, when ε is sufficiently small, the times of breakdown in the calculations involving the gentler wave are different for different orders of backward differencing. It can be seen that the failures that arise when using four or five orders are consistent with the "steep-wave" type of breakdown identified in Table IV. However, possibly because this form of breakdown is very slow for such a gentle wave, another form of instability has time to grow and to destroy the calculations at an earlier stage when two or three orders of backward differencing are used. This "weak instability" appears to emerge only at these orders of backward differencing, and to be not as much affected by the wave amplitude as the "steep-wave" instability, which predominates at large enough wave-amplitudes.

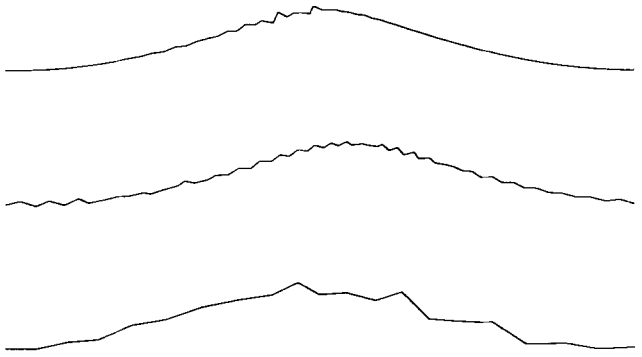

FIG. 7. Wave profiles shortly before breakdown due to (from top to bottom): (a) a strong numerical instability; (b) a steep-wave numerical instability; and (c) a weak numerical instability (details in the text). The top two profiles are plotted at their natural scale while the bottom profile is vertically exaggerated by the factor three.

Some of the reasons for the appearance of these instabilities, including their dependence on time-step size, point density and order of backward differencing, are presented later in this section. However, in order to *illustrate* the natures of these instabilities more satisfactorily, surface profiles from three different calculations are plotted in Fig. 7. Using 60 surface points, $\varepsilon = 10^{-4}$, fifth-order backward differencing and the same wave with $ak = 0.3$, profiles just before breakdown are presented in Fig. 7a (showing a case of the strong instability after only 15 time-steps, or 1 $\frac{1}{4}$ wave periods) and in Fig. 7b (showing the steep-wave instability after 13 $\frac{1}{4}$ periods). Using two orders of backward differencing and 20 surface points with $\varepsilon = 10^{-4}$, a case of the weak instability, arising for the wave of amplitude $ak = 0.1$, is presented in Fig. 7c after 550 wave periods.

All three wave profiles display a "sawtooth" character, with successive points either raised or lowered. However, the range of sawtooth behaviour appears to be almost uniform in the cases of the steep-wave and weak instabilities, while it is very localised behind the crest of the wave (which propagates from left to right) in the case of the strong instability. The pictures clearly result from a production of predominantly "sawtooth" disturbances. With the strong instability, these appear to emerge spontaneously, especially from the region of the crest.

7.2. Effect of Smoothing

From the examinations above, it seems clear that the strong instability can be eliminated simply by ensuring that time-steps remain sufficiently small; the weak instability is eliminated by selecting either four or five orders of backward differencing (rather than two or three). However, the steep-wave instability always appears to be present, regardless of the number of points, the amplitude of the basic steady wave, the order of backward differencing, or the value of the precision control parameter ε. Because of this, it presents a fundamental difficulty in calculating asymptotically long-time evolutions. Many of the calculations presented above can be seen to survive for very many wave periods with no obvious sign of any difficulty. Thus, the instability may not present a significant problem for calculations over sufficiently limited time-scales, which can always be lengthened by suitably reducing ε. The calculations presented in Section 5 are all of this nature.

Nevertheless, the difficulty still remains. Any perfectly steady "stable" wave (in the sense that it does not suffer from a normal mode instability) should be expected, in principle, to be able to propagate unchanged indefinitely—a property that the numerical scheme is clearly unable to reproduce without further adjustments.

One possible adjustment is the use of "smoothing," the effect of which is simply to remove very short wave-modes, having a wavelength of about two grid points. Using a highly selective 15-point "sawtooth" smoothing formula (described in Appendices B and C), to smooth the values of $\mathbf{R}(\xi, t)$ and $\Phi(\xi, t)$ *after every time-step*, the situation is almost completely recovered as seen in Fig. 8. Taking a total of 60 points, setting $\varepsilon = 10^{-4}$ and $l_B = 5$, and using the routines described in Appendix B to ensure conservation of mean level and total energy, the large wave of amplitude $ak = 0.42$ was followed for a total of *4000 wave-periods*! By contrast, the calculation of the same wave under the same conditions without smoothing broke down after only 13 $\frac{1}{4}$ phase periods. A Fourier decomposition of the resulting calculated wave profile at every hundredth period is shown in Fig. 8. Because the most significant modes in the wave decomposition remain practically constant, it is readily seen from this that the wave profile is substantially preserved. Remarkably, the overall error in phase-speed in this extensive calculation was no more than 10^{-6}%. Some energy is, nevertheless, transferred into short wavelength modes which seem to persist indefinitely. Their amplitude is, however, relatively small at between about 0.0002% and 0.0008% of the basic wave amplitude.

It may be noted that when the strong numerical instability is not present (as in this calculation), it should not strictly be necessary to smooth the surface data at every time-step in order to stabilise the wave—disturbances grow very slowly and take many time-steps to accumulate. However, the 15-point formula is so selective in destroying only short wavelength modes that its much more frequent (and even repeated) use makes very little difference in such a calculation. Smoothing does, however, make a major difference in controlling the appearance of the strong numerical instability.

More general aspects of smoothing are discussed further in Appendix B.

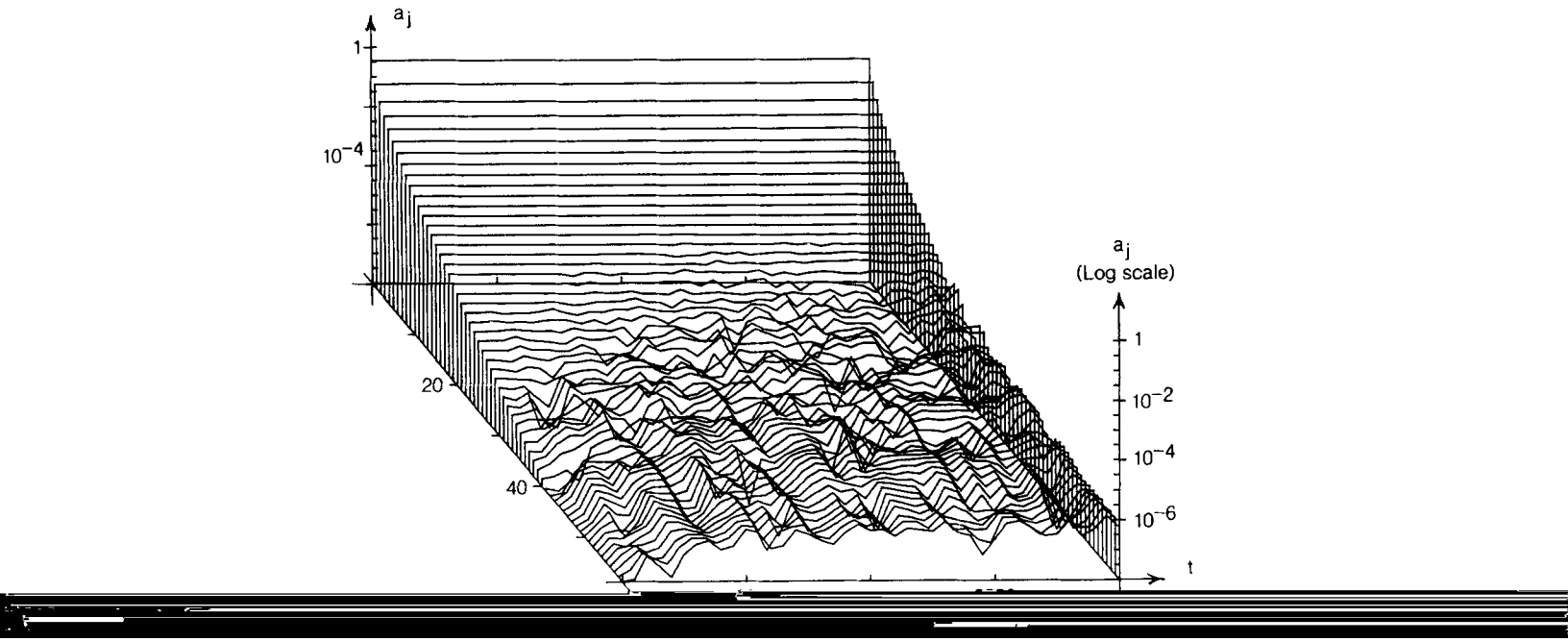

FIG. 8. Amplitudes of the Fourier components a_j of a wave of steepness $ak = 0.42$ plotted at every 100 wave-periods in an evolution lasting 4000 periods.

7.3. Analysis of the Rôle of Explicit Time-Stepping

Some insight into the nature of the instabilities that have been identified can be obtained by examining the effect of the method of time-stepping. Together with the numerical dispersion relation discussed in Section 6.1, this analysis reveals the linear stability of the numerical method for a flat horizontal surface.

7.3.1. *Model Problem*

The effect of time-stepping is most easily examined by considering a model situation. Let us suppose that a linear time-periodic wave-mode $y = y_0 = \exp[i(\omega t - kx)]$ is present at a time $t = 0$, so that calculated derivatives at this time are precisely

$$\begin{aligned} y_t &= i\omega y_0, \\ y_{tt} &= -\omega^2 y_0, \\ y_{ttt} &= -i\omega^3 y_0, \end{aligned} \tag{7.1}$$

etc. This would, for example, model waves of very small amplitude on an otherwise flat horizontal surface or, at least asymptotically, on a surface that changes over length and time-scale scales that are very much longer than the wavelength and period of the model wave. The *numerically time-stepped* evolution of y may be taken to behave differently, adopting the form

$$y = \exp[(\gamma + i)\,\omega t - ikx], \tag{7.2}$$

in which the values of y are calculated only at successive times incremented by, say, δt (for a constant size of time-step) and in which a numerical growth-rate eigenvalue γ is taken into account. Derivatives at each time-step, however, may be taken to be calculated "accurately" as in Eq. (7.1).

This mimics many aspects of the full numerical algorithm presented here in which the three derivatives (7.1) are calculated without reference to any previous data, and so are independent of the size of time-step. For sufficiently short waves, down to a wavelength of two grid points, the relevant value of ω may be taken to be known from the numerical dispersion relation in Fig. 6. A full linear stability analysis of the algorithm on a flat surface in deep water would produce exactly the same dispersion relation for vanishingly small time-steps. The linear stability for non-vanishing time-steps, with high-order time-stepping based on direct calculation of the first three derivatives and various possible orders of backward differencing, can then be separated into an analysis of Eqs. (7.1) and (7.2). Also, although the analyses that follow are based on constant time-steps, they could be extended to consider arbitrary sizes of time-step (at the cost of greater complexity). Typically however, time-steps in the numerical scheme do indeed vary little from one step to the next so that this is not likely to be particularly valuable.

To begin with, it is easily seen that a straightforward truncated Taylor series, based only on the "exact" derivatives (7.1), produces a growth-rate eigenvalue γ given by

$$e^{(\gamma+i)\lambda} = \left(1 - \frac{\lambda^2}{2!} + \cdots + (-1)^{l/2}\frac{\lambda^l}{l!}\right) + i\left(\lambda - \frac{\lambda^3}{3!} + \cdots + (-1)^{(m-1)/2}\frac{\lambda^m}{m!}\right), \tag{7.3}$$

where the order of truncation is either the even number l (with $m = l - 1$) or the odd number m (with $l = m - 1$), and in which λ represents a normalised size of time-step, $\lambda = \omega\,\delta t$.

Using three directly calculated derivatives (as implemented in the numerical algorithm) and, for example, appropriate formulae for second-order backward differencing based on the two previously calculated third derivatives at $t = -\delta t$ and $t = -2\,\delta t$, leads to the following formula for the growth-rate,

$$\mu = 1 + i\lambda - \frac{\lambda^2}{2!} - i\frac{\lambda^3}{3!} - i\frac{\lambda^4}{4!}\frac{3 - 4/\mu + 1/\mu^2}{2\lambda} - i\frac{\lambda^5}{5!}\frac{1 - 2/\mu + 1/\mu^2}{\lambda^2}, \tag{7.4}$$

in which we have set $\mu = \exp[(\gamma + i)\,\omega\,\delta t]$. Since the basic wave is amplified by the complex factor of μ from its current value at each successive time-step, the role of backward differencing in this formula can be seen to appear via the terms containing $1/\mu$ and $1/\mu^2$. These correspond to the "numerical" (and possibly inexact) magnitudes of the basic wave at the two previous time-steps. The last two terms in Eq. (7.4) respectively represent fourth and fifth derivative contributions to the Taylor series based on a polynomial fit to the values of the third derivative at these and the current time.

Formulae for the growth-rate factor μ using different orders of backward differencing can be obtained in a completely analogous way. Expressing the results in terms of polynomials in μ, the formulae for the growth-rates obtained using orders of backward differencing from zero to five can be written as

$$\begin{aligned}
\mu &= 1 - \frac{\lambda^2}{2} + i\left(\lambda - \frac{\lambda^3}{6}\right)\\
\mu^2 &= \mu\left[1 - \frac{\lambda^2}{2} + i\left(\lambda - \frac{5}{24}\lambda^3\right)\right] + i\frac{1}{24}\lambda^3\\
\mu^3 &= \mu^2\left[1 - \frac{\lambda^2}{2} + i\left(\lambda - \frac{19}{80}\lambda^3\right)\right] + i\mu\frac{1}{10}\lambda^3 - i\frac{7}{240}\lambda^3\\
\mu^4 &= \mu^3\left[1 - \frac{\lambda^2}{2} + i\left(\lambda - \frac{47}{180}\lambda^3\right)\right] + i\mu^2\frac{41}{240}\lambda^3 - i\mu\frac{1}{10}\lambda^3 + i\frac{17}{720}\lambda^3\\
\mu^5 &= \mu^4\left[1 - \frac{\lambda^2}{2} + i\left(\lambda - \frac{2837}{10080}\lambda^3\right)\right] + i\mu^3\frac{1271}{5040}\lambda^3 - i\mu^2\frac{373}{1680}\lambda^3 + i\mu\frac{529}{5040}\lambda^3 - i\frac{41}{2016}\lambda^3\\
\mu^6 &= \mu^5\left[1 - \frac{\lambda^2}{2} + i\left(\lambda - \frac{12079}{40320}\lambda^3\right)\right] + i\mu^4\frac{13823}{40320}\lambda^3 - i\mu^3\frac{8131}{20160}\lambda^3 + i\mu^2\frac{5771}{20160}\lambda^3\\
&\quad - i\mu\frac{895}{8064}\lambda^3 + i\frac{731}{40320}\lambda^3,
\end{aligned} \tag{7.5}$$

respectively. Apart from the first, which has only one-solution, these formulae possess multiple complex roots for $\mu(\lambda)$. Of these, any root which gives $|\mu| > 1$ or $\mathrm{Re}(\gamma) > 0$ represents a progressive growth in the numerically calculated magnitude of the function y that is being modelled. It therefore indicates the presence of a numerical instability.

Strong Instability. The solution of most interest therefore, is the solution with the largest value of $\mathrm{Re}(\gamma)$. Accordingly, maximum values of $\mathrm{Re}(\gamma)$ are plotted in Fig. 9

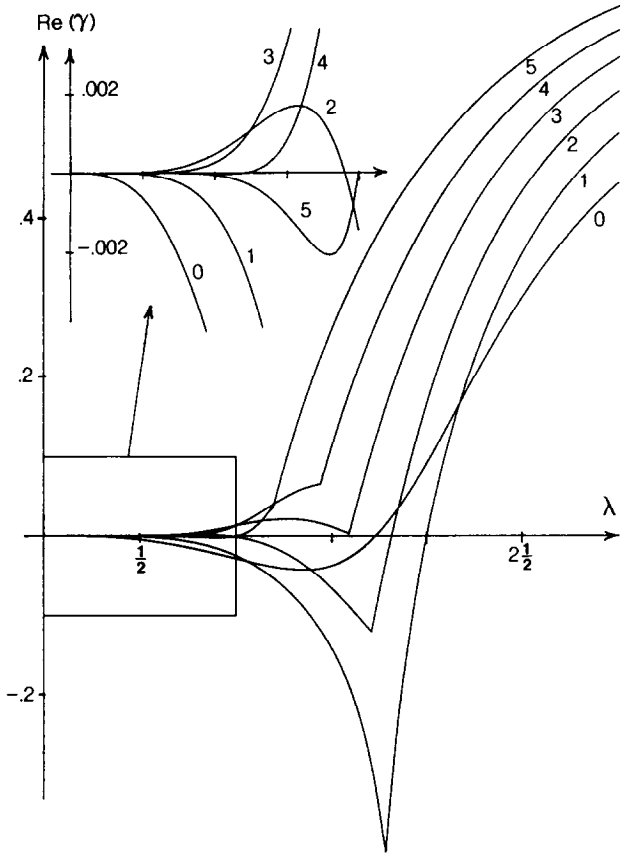

FIG. 9. Maximum real parts of the growth-rate eigenvalue $\gamma(\lambda)$ for levels of backward differencing between zero and five.

as a function of the time-step parameter λ. This shows clearly that all orders of backward differencing produce a fairly large positive value of $\mathrm{Re}(\gamma)$ at sufficiently large time-steps. This accounts for the appearance of the strong instability in the wave calculations above. In all cases, the root of the relevant equation in (7.5) that produces this instability becomes stable again as λ decreases below a strong instability threshold value of $\lambda^{s}_{l_B}$, where

$$\begin{aligned} &\lambda^{S}_{0} \approx 1.732, \quad \lambda^{S}_{1} = 2, \quad \lambda^{S}_{2} \approx 1.818, \\ &\lambda^{S}_{3} \approx 1.590, \quad \lambda^{S}_{4} \approx 1.366, \quad \lambda^{S}_{5} \approx 1.156. \end{aligned} \tag{7.6}$$

Because $\lambda^{S}_{l_B}$ decreases as l_B increases (excluding $l_B = 0$), and because values of $\mathrm{Re}(\gamma)$ increase with l_B above this threshold, this also accounts for the fact that the strong instability tends to be felt sooner (that is, at smaller values of ε) and to grow more rapidly for larger orders of backward differencing, as seen in Table V.

Accuracy and Weak Instability. Except when $l_B = 0$, another root takes over in determining the maximum value of $\mathrm{Re}(\gamma)$ as λ continues to decrease. In all cases, the values of $\gamma(\lambda)$ corresponding to this root decrease to zero as λ tends to zero, indicating that the "numerical" time-stepping procedure would indeed asymptotically reproduce the correct behaviour for y (as it should do) in the limit of very small time-steps. One finds that the magnitude of $|\gamma(\lambda)|$ increases in proportion to λ^{3+l_B} when λ is very near zero, thus reflecting the order of accuracy of the basic time-stepping procedures. More specifically, near $\lambda = 0$, one actually finds that $\mathrm{Re}(\gamma)$ increases in proportion to $\lambda^{3+2[l_B/2]}$ and that $\mathrm{Im}(\gamma)$ increases in proportion to $\lambda^{4+2[l_B/2]}$, where $[l_B/2]$ represents the largest integer less than or equal to $l_B/2$. This tends to indicate that errors due to time-stepping arise predominantly in reproducing the phase of a wave for even orders of backward differencing, and in reproducing the amplitude for odd orders.

However, the sign of $\mathrm{Re}(\gamma)$ is not always found to be negative when λ is small. The inset in Fig. 9 shows how it becomes positive, in any neighbourhood of the origin, for both second and third orders of backward differencing. With $l_B = 2$, $\mathrm{Re}(\gamma)$ does become negative again, showing the existence of a *window of stability* that does not include the origin. With three orders of backward differencing, the real part of this root does not become negative before the more strongly unstable root takes over, indicating that a time-stepping procedure based on $l_B = 3$ would be uniformly unstable for any positive time-step. In a wave surface involving many possible modes, there is typically a distribution of frequencies ω, with the longer wavelengths tending to have smaller values of ω. Thus some modes, at least, will always tend to lie in the regions of weak instability. Most particularly, because the regions of instability include any small neighbourhood of the origin, an eventual numerical growth cannot be eliminated (although it can be delayed) by taking reduced time-steps. Moreover, for small enough time-steps, it is the highest frequency (or shortest) waves that would tend to grow most quickly.

For other orders of backward differencing, a single window of stability that extends to the origin is predicted by the solutions of Eqs. (7.5) so that, at least with four and five orders of backward differencing, one would not expect to find an unstable numerical growth for small enough sizes of time-step. Once again, this finding is in accordance with the observations based on Table V, that an instability is observed much sooner for l_B equal to two or three when ε and ak are sufficiently small.

Still considering the roots that account for weakly unstable behaviour, some of the real parts of $\gamma(\lambda)$ change sign at specific values of λ. Denoting these values by $\lambda^{W}_{l_B}$, one finds

$$\begin{aligned} &\lambda^{W}_{0} \approx 1.732^{*}, \quad \lambda^{W}_{2} \approx 0.952, \quad \lambda^{W}_{3} \approx 1.620, \\ &\lambda^{W}_{4} \approx 0.604^{*}, \quad \lambda^{W}_{5} \approx 1.001^{*}. \end{aligned} \tag{7.7}$$

Those values that are written with an asterisk represent points at which $\mathrm{Re}(\gamma)$ increases as λ increases through $\lambda^{W}_{l_B}$. These values are most significant in the cases with $l_B = 4$ or 5, when they represent genuine instability thresholds above which a weak instability appears before the strong instability thresholds $\lambda^{S}_{l_B}$ are reached. Because λ^{W}_{5} is greater than λ^{W}_{4}, it follows that calculations are stable to the weak form of instability over a wider range of λ when performed using five rather than four orders of backward differencing.

7.3.2. *Application to Sawtooth and m-Point Instability Thresholds*

The actual evolution of infinitesimal disturbances on a moving wave surface is more difficult to predict. However the analysis above for a flat-surface does bear some generalisation. A local point separation δr is easily identified with $|\mathbf{R}_\xi|$ and a local equivalent of gravity g is the normal pressure gradient P_n at the surface—which is the normal component of $\nabla P = \rho(D\mathbf{u}/Dt + g\hat{\mathbf{j}})$. If changes in the overall wave motion are considered to take place relatively slowly, over many surface points, then one can expect the analysis above at least partly to apply, predicting weak or strong numerical instabilities that depend on the *local* surface properties.

Considering a small disturbance mode to have a wavelength of m surface points, it is readily seen that this corresponds to a wavenumber of $k_m = 2\pi/|m\mathbf{R}_\xi|$. According to linear theory, this wave should have a frequency of $(P_n k_m)^{1/2}$ (being the surface equivalent of $\sqrt{gk}$). However

taking into account the numerical dispersion relation of Fig. 6, one should find instead that

$$\omega_m \approx \sqrt{P_n/|\mathbf{R}_\xi|} \times \begin{cases} 1.474 & : m = 2 \\ 1.404 & : m = 3 \\ 1.25\sqrt{4/m} & : m \geq 4 \end{cases} \quad (7.8)$$

at least for the methods of estimating derivatives and the method of solving Laplace's equation used in this implementation of the algorithm. For a given (say, threshold) value of λ, the time-step size δt corresponding to

$$\delta t = \lambda/\omega_m \approx \lambda \sqrt{|\mathbf{R}_\xi|/P_n} \times \begin{cases} 0.678 & : m = 2 \\ 0.712 & : m = 3 \\ 0.80\sqrt{m/4} & : m \geq 4. \end{cases} \quad (7.9)$$

Given a wave motion involving changing values of P_n and $\mathbf{R}_\xi$, this formula allows one to estimate the size of time step that would, for example, make a sawtooth mode ($m = 2$) become unstable at some point. For instance, with fifth order backward differencing, one would need to set $\lambda = \lambda_5^W \approx 1$ in equation (7.9) which would then provide a threshold size of time step below which all weak and strong instabilities would be absent.

In order to check the results of the model stability analysis, some numerical tests were performed using only two or three very slightly disturbed grid points in a spatial period. The imposed periodicity then ensures that only a sawtooth mode ($m = 2$) or three-point periodic mode ($m = 3$), respectively, is able to develop—these being the only possible modes for these numbers of points. By following the growth of disturbances using two orders of backward differencing and fixed sizes of time-step, a numerical estimate was made of the values of the growth-rate eigenvalue $\mathrm{Re}(\gamma)$. The results of these calculations are presented in Fig. 10 as a function of the time step δt, with dotted curves representing growth-rates predicted from the model analysis. The agreement between the theoretical predictions and the numerical estimates is very good, especially considering that the numerical estimates of the decay rates (in particular) were difficult to obtain accurately.

The information shown in the figure is scaled as if these sawtooth and 3-point periodic modes were developing on a flat surface represented by any number of spatial points in a periodic domain with equation (7.9) providing the appropriate scalings between λ and δt for the model predictions. In this way, the diagram provides a direct indication of the levels of time-step at which the first two short-wavelength modes pass through stability boundaries when using two orders of backward differencing.

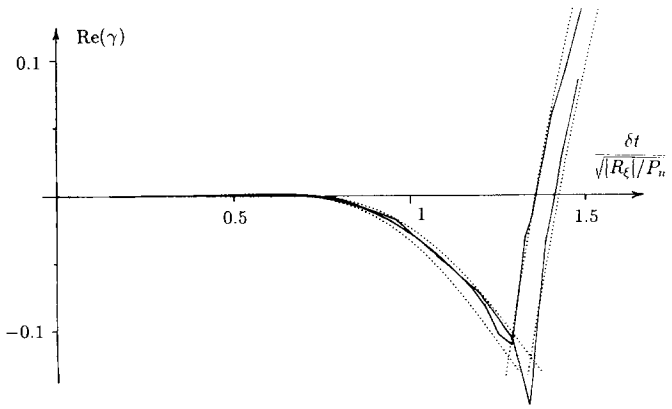

FIG. 10. Numerically estimated and theoretical (shown dotted) growth-rates $\mathrm{Re}(\gamma)$ when two orders of backward differencing are used. These are plotted as functions of time-step for 2-point (sawtooth) and 3-point modes of instability on a fluid surface.

7.4. Steep-Wave Instability

As observed in connection with Table IV, the steep-wave instability seems to be associated with the curvature and normal pressure gradient at the crest of a wave. On the other hand, being related most directly to small perturbations on an otherwise flat surface, with no direct consideration of spatial variation and wave propagation, the model analysis above does not seem to be able to predict anything significant about the nature and growth of this type of instability, which still awaits an adequate explanation.

One may only conjecture at this stage that it might be associated with the near zero group velocity found for a significant range of wave-modes near the sawtooth or two-point limit (from the numerical dispersion relation in Fig. 6) and some genuinely nonlinear interaction between such modes and properties associated with steep wave-crests. Given that a near sawtooth wave-mode has a group velocity that is practically zero, a localised disturbance on this scale in the surface tends to remain fixed with respect to surface particles and to be unable to disperse. For all practical purposes it behaves like a localised standing-wave which should, in principle, radiate its energy at the group velocities of its component wave-modes.

It seems a likely possibility that a nonlinear interaction with a wave-crest could amplify this disturbance slightly each time the crest passes through it (at about every particle-period), leading to a buildup of energy in short wave-modes that remains more-or-less fixed to the Lagrangean numerical grid points. Indeed, being more sharply curved than any other part of a wave surface, a steep wave-crest contains more shorter wave components. The difficulty over numerically modelling the group velocities of these components may mean that they are simply stripped away from the crest as it passes repeatedly through the grid.

7.5. Stabilising the Algorithm

To conclude the findings of this discussion on stability, the linear stability analysis backs up the numerical findings that a strong instability is eliminated by restricting the maximum size of time-step. Equation (7.9) gives this time step limit where λ takes an appropriate value $\lambda^{S}_{l_B}$ given in (7.6). The weak instability is eliminated by taking l_B to equal 4 or 5 and by restricting time-steps with $\lambda = \lambda^{W}_{l_B}$ in Eq. (7.9). Should the remaining (steep-wave) instability prove a problem, it can be eliminated using very selective smoothing formulae discussed in Appendices B and C.

It is worth noting that the linear stability analysis of Section 7.3.1 depends only on the method for time-stepping and not on the method of solving Laplace's equation. The latter affects only the calculated value of ω in this analysis. The same findings (relating to the presence of "weak" and "strong" instabilities) would thus apply to any method which uses the same principle of calculating higher time derivatives and time-stepping using truncated Taylor series. The "steep-wave" instability may be a product of the method for solving Laplace's equation, and other techniques may introduce yet further instabilities.

8. CONCLUSIONS

Steep gravity-wave phenomena, and indeed fluid surface and interface problems in general, present a rich range of steady or unsteady behaviour that is often difficult to model analytically. In such cases, reliable numerical calculations can provide both interesting and practically valuable information that cannot be obtained in any other theoretical way.

The algorithm that has been presented in this paper offers and tests some useful means of enhancing the accuracy and speed of existing methods for numerically simulating the movement of wave surfaces on two-dimensional fluids. This is mainly achieved by using direct calculation of a number of time-derivatives of the surface motion and finds a further contribution from using high-order methods for calculating spatial or arclength derivatives. Using the latter, the calculations presented in this paper demonstrate that surprisingly few numerical "surface" points can lead to high degrees of computational accuracy.

Extensive tests of an implementation of the algorithm (using Cauchy's integral theorem in order to solve iteratively the fluid boundary-value problem for up to three time-derivatives) are reported in this paper. They reveal some signs of three identifiable forms of numerical instability that have been closely examined both by using appropriate test-runs and by a model stability analysis. These examinations show how a reliably stable numerical scheme is produced by adjusting the method to remove all signs of instability.

It is found that two of these instabilities are eliminated by making appropriate restrictions on the maximum size of time-step and by using four or five, rather than two or three, orders of backward differencing to improve the accuracy of time-stepping. These instabilities would be present using any technique (including Cauchy's integral theorem) for solving Laplace's equation. The third instability is conjectured to be related to inaccuracies in numerically simulating the group velocity of very short wave-modes, near the numerical limit of two points per wavelength—it is also very dependent on the steepness of the waves in the wave-surface. Should it become necessary, it is convincingly demonstrated that this (and indeed the other two forms of numerical instability) can be completely controlled by using very selective, high order, smoothing formulae. In many practical circumstances however, these instabilities are found to play no significant rôle.

This numerical scheme is found to be able to calculate many complicated surface simulations very accurately and very quickly indeed. As a result, only modest computing resources need be required for the investigation of many surface phenomena. Of course, with powerful computers, this means that it is also now possible to investigate increasingly ambitious problems.

APPENDIX A: CALCULATION OF HIGHER TIME DERIVATIVES

In order to be able to solve equations (2.10) for the gradients of ϕ_t, ϕ_{tt}, etc., it is first of all necessary to know the values of ϕ_t, ϕ_{tt} etc. on the surface. Rewriting Bernoulli's equation (2.7) in Eulerian form gives

$$\phi_t + \mathbf{u}^2/2 + P/\rho + gy = 0. \tag{A.1}$$

Rearranging this and successively differentiating shows that

$$\begin{aligned} \phi_t &= -[P/\rho + gy + \mathbf{u}^2/2] \\ \phi_{tt} &= -[P_t/\rho + \mathbf{u}\cdot\mathbf{u}_t] \\ \phi_{ttt} &= -[P_{tt}/\rho + \mathbf{u}\cdot\mathbf{u}_{tt} + \mathbf{u}_t\cdot\mathbf{u}_t], \end{aligned} \tag{A.2}$$

etc., which give the required surface values in terms of lower order Eulerian time-derivatives of P and $\mathbf{u}$.

However, the pressure P is only open to definition on the surface $\mathbf{R}(\xi, t)$ which is moving with time. Thus while the Lagrangean derivatives DP/Dt, D^2P/Dt^2, etc., can be specified, the time-derivatives of P at fixed values of x and y (i.e. the Eulerian derivatives, P_t, P_{tt}, etc.) cannot, in general, be specified directly. To get over this problem, a conversion from Eulerian to Lagrangean derivatives has to be made as follows,

$$P_t = \frac{DP}{Dt} - \mathbf{u}\cdot\nabla P = \frac{DP}{Dt} + \rho\mathbf{u}\cdot[\mathbf{u}_t + \nabla(\mathbf{u}^2/2 + gy)]$$
$$= \frac{DP}{Dt} + \rho\mathbf{u}\cdot\left[\frac{D\mathbf{u}}{Dt} + g\hat{\mathbf{j}}\right]$$
$$P_{tt} = \frac{D^2P}{Dt^2} - \mathbf{u}\cdot\nabla P_t - \frac{D}{Dt}(\mathbf{u}\cdot\nabla P) \tag{A.3}$$
$$= \frac{D^2P}{Dt^2} + \rho\mathbf{u}\cdot[\mathbf{u}_{tt} + \nabla(\mathbf{u}\cdot\mathbf{u}_t)] + \rho\frac{D}{Dt}\left[\mathbf{u}\cdot\left(\frac{D\mathbf{u}}{Dt} + g\hat{\mathbf{j}}\right)\right],$$

etc., where $\hat{\mathbf{j}}$ is the vertical unit vector $\hat{\mathbf{j}} = \nabla y$. In these expressions, terms such as ∇P and ∇P_t have been eliminated by using the relations,

$$\mathbf{u}_t = -\nabla(P/\rho + gy + \mathbf{u}^2/2)$$
$$\mathbf{u}_{tt} = -\nabla(P_t/\rho + \mathbf{u}\cdot\mathbf{u}_t), \tag{A.4}$$

etc., obtained by combining equations (2.10) and (A.2).

It can thus be seen that the required *surface* values for ϕ_t, ϕ_{tt}, etc., are given by

$$\phi_t = -\{P/\rho + gy + \mathbf{u}^2/2\}$$
$$\phi_{tt} = -\left\{\frac{DP}{Dt}\Big/\rho + \mathbf{u}\cdot\left(\frac{D\mathbf{u}}{Dt} + \mathbf{u}_t + g\hat{\mathbf{j}}\right)\right\}$$
$$\phi_{ttt} = -\left\{\frac{D^2P}{Dt^2}\Big/\rho + \mathbf{u}\cdot\left[\frac{D^2\mathbf{u}}{Dt^2} + 2\mathbf{u}_{tt} + \nabla(\mathbf{u}\cdot\mathbf{u}_t)\right]\right. \tag{A.5}$$
$$\left. + \mathbf{u}_t^2 + \frac{D\mathbf{u}}{Dt}\cdot\left(\frac{D\mathbf{u}}{Dt} + g\hat{\mathbf{j}}\right)\right\},$$

etc., on $\mathbf{r} = \mathbf{R}(\xi, t)$, where $P(\mathbf{R}, t)$ is open to definition (thereby specifying DP/Dt, D^2P/Dt^2, etc., in the process) —for a constant surface pressure all of the derivatives, DP/Dt, D^2P/Dt^2, etc., will simply be zero.

Before the surface values can be calculated in Eqs. (A.5), it is necessary to evaluate the appropriate Lagrangian derivatives of the velocity at the surface. These are also needed for time-stepping the surface position. The following relations hold between the Eulerian and Lagrangian

$$\frac{D\mathbf{u}}{Dt} = \mathbf{u}_t + (\mathbf{u}\cdot\nabla)\mathbf{u}$$
$$\frac{D^2\mathbf{u}}{Dt^2} = \mathbf{u}_{tt} + 2(\mathbf{u}\cdot\nabla)\mathbf{u}_t + (\mathbf{u}_t\cdot\nabla)\mathbf{u} + (\mathbf{u}\cdot\nabla)^2\mathbf{u}, \tag{A.6}$$

etc. In order to use these relations, the various gradient terms must be evaluated. This can be done by noting that for $\mathbf{u} = (u, v)$,

$$u_x + v_y = 0 = u_y - v_x \tag{A.7}$$

so that if $\mathbf{u} = (U(\xi, t), V(\xi, t))$ at the surface,

$$u_x = -v_y = (U_\xi X_\xi - V_\xi Y_\xi)/(X_\xi^2 + Y_\xi^2)$$
$$v_x = u_y = (U_\xi Y_\xi + V_\xi X_\xi)/(X_\xi^2 + Y_\xi^2). \tag{A.8}$$

Exactly analogous expressions can be used to evaluate the gradient of any of the derivatives of $\mathbf{u}$, such as $\mathbf{u}_t$, $\mathbf{u}_x$, $\mathbf{u}_{yt}$, given only their values on the surface. In this way it is possible to evaluate all of the terms required for evaluating Eqs. (A.5) and the transformations (A.6). For example:

$$(\mathbf{u}_t\cdot\nabla)\mathbf{u} = \left(u_t\frac{\partial}{\partial x} + v_t\frac{\partial}{\partial y}\right)(u, v)$$
$$= (u_t u_x + v_t v_x,\ u_t v_x - v_t u_x)$$

and (A.9)

$$(\mathbf{u}\cdot\nabla)^2\mathbf{u} = \left(u\frac{\partial}{\partial x} + v\frac{\partial}{\partial y}\right)\left(u\frac{\partial}{\partial x} + v\frac{\partial}{\partial y}\right)(u, v)$$
$$= (u_x^2 + v_x^2)(u, v) + (u^2 - v^2)(u_{xx}, v_{xx})$$
$$+ 2uv(v_{xx}, -u_{xx}).$$

With these equations (continued to still higher derivatives if necessary) and some means of solving Laplace's equation, it becomes possible successively to calculate up to any order of time-derivative of velocity. In order to set up Taylor series in time for the surface profile $\mathbf{R}$ and surface potential Φ, it only remains to extend Eqs. (2.6) and (2.7) by straightforward differentiation, so that

$$\mathbf{R}_t(\xi, t) = \frac{D\mathbf{r}}{Dt} = \mathbf{u}, \qquad \mathbf{R}_{tt}(\xi, t) = \frac{D^2\mathbf{r}}{Dt^2} = \frac{D\mathbf{u}}{Dt}, \text{ etc.} \tag{A.10}$$

and

$$\Phi_t(\xi, t) = \frac{D\Phi}{Dt} = \mathbf{u}^2/2 - (P/\rho + gy)$$
$$\Phi_{tt}(\xi, t) = \frac{D^2\Phi}{Dt^2} = \mathbf{u}\cdot\frac{D\mathbf{u}}{Dt} - \left(\frac{DP}{Dt}\Big/\rho + gV\right) \tag{A.11}$$

etc., where ξ is held fixed in the differentiation of $\mathbf{R}$ and Φ

APPENDIX B: PROCEDURES FOR MANIPULATING THE SURFACE DATA

In order to make better use of the program in some circumstances two additional features were introduced to modify the surface data in specific ways:

B.1. Smoothing

As seen in Section 7.2, smoothing may be used occasionally as one means of removing some signs of numerical

instability. Provided the surface is described by a sufficiently large number of points, it also may be thought of as a means of helping to maintain accuracy. This is achieved either because smoothing selectively removes modes with wavelengths as short as two or three grid points (which are least accurately modelled according to the dispersion relation in Fig. 6) or because it helps to ensure a "smooth" point distribution (which is necessary if point label derivatives are to be calculated accurately).

Five and seven point formulae, designed to destroy "sawtooth" oscillations in surface data, were derived by Longuet-Higgins and Cokelet [2]. It was decided to extend this approach by also allowing for 7-,[4] 9-, 11-, 13-, and 15-point formulae as presented in Appendix C. The higher-order sawtooth smoothing formulae are found to be much more selective than lower-order formulae in destroying only data that represent a successively positive and negative displacement from otherwise "smooth" values As a result they cause disproportionately less damage to other modes each time they are used. Two formulae are also derived that are designed to destroy both sawtooth oscillations (having a periodicity of two points) and oscillations that are periodic over every three data points.

Figure 11a shows the result of using each one of these formulae to "smooth" sinusoidally varying data discretised using differing numbers of points per wavelength. With only two points, the wave is a pure zig-zag and is completely destroyed in all cases. With four points per wavelength, the 11-point sawtooth smoothing formula reduces the amplitude of the data by about 3% as compared with the 25% of the 5-point formula and 0.8% of the 15-point formula. The formulae designed also to remove 3-point oscillations completely destroy waves with three points per wavelength (as they should), and decreasingly alter waves with more points. In this, the formula based on 15 points is less severe than the formula based on 9 points.

In fact, the higher-order sawtooth formulae are found to cause so little loss of accuracy that they can be used more frequently (even repeatedly) and so be more effective at destroying any nearly zig-zag or 3-point periodic component while still causing less overall damage to anything else. The effect of repeatedly using the 15-point sawtooth formula is shown in Fig. 11b, in which it can be seen that many successive applications to sinusoidal data tend to selectively remove modes over a very limited range of wavelengths.

Noting from Tables I and II that the total energy usually proves to be a sensitively affected property of a wave when N and ε are varied, the effect of using various smoothing formulae on the total energy was tested using a wave of amplitude $ak = 0.4$. For differing numbers of points used to discretise the wave surface, the relative change in total energy resulting from a single use of each smoothing formula on all of the functions X, Y, and Φ is shown in Table VI.

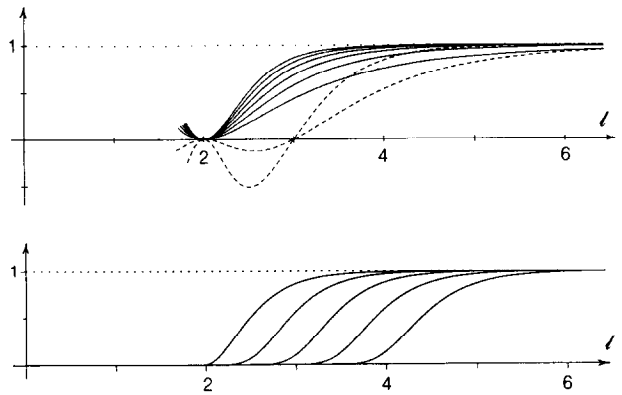

FIG. 11. (a) Resulting wave amplitude after smoothing sinusoidal data with l points per wavelength using sawtooth (solid lines) and both sawtooth and 3-point periodic (dashed lines) smoothing formulae—Eqs. (C.11) and (C.13); (b) (lower diagram) Amplitudes of the same initial data after 1, 4, 16, 64 and 256 repeated applications of the 15-point "sawtooth" formula.

The observable change in total energy becomes very small with the higher-order formulae when the wave is described by a moderately large number of points. When this is the case, repeated applications of the smoothing formulae make a diminishing difference to the wave so that the effect is not arithmetically cumulative and many smoothing passes tend to result in about the same order of magnitude of change as a single pass. Smaller amplitude waves are even less significantly affected. It can also be seen from Table VI that the 9- and 15-point sawtooth and 3-point periodic smoothing formulae have a more dramatic effect than their sawtooth counterparts. Because these formulae approach asymptotically the sawtooth formulae based on 5 and 9 points, respectively (as in Fig. 11a), their repeated application tends to behave in exactly the same way as these sawtooth formulae.

B.2. Conservation of Energy and Mean-Surface Level

The Taylor-series time stepping procedure does not explicitly conserve energy and the mean surface level. Any changes in these values per wave period are found to be small, provided ε is small, and may be used as a measure of the overall accuracy of any results (as in Section 6). However, it is also possible to modify the time-stepping procedure in order to ensure conservation of these quantities. This is desirable under some circumstances, particularly when calculations are made over many wave-periods. In such calculations, it would be convenient to use the same value of ε as would be acceptable for calculating over a shorter time-scale. Unfortunately, the error in calculating the energy (in particular) tends to accumulate so that,

[4] The seven-point formula used here is different from that used by Longuet-Higgins and Cokelet.

TABLE VI

Percentage Change in Calculated Total Energy Resulting From a Single Use of a Sawtooth (2-Point Periodic) or Sawtooth and 3-Point Periodic Smoothing Formula on a Wave of Height $ak = 0.4$ Described by Differing Numbers of Surface Points

Number of points	Calculated energy	Number of points in sawtooth smoothing formula						2 and 3 point modes	
		5	7	9	11	13	15	9	15
4	0.4373540	−43.9	−23.26	−22.562	−11.483	−7.1024	−3.2125	−92.04	−58.635
5	0.4399875	−23.1	−8.401	−5.7877	−2.0246	−1.0354	−0.34744	−57.57	−10.919
6	0.4401338	−12.4	−3.117	−1.4759	−0.29248	−0.01843	0.05582	−28.86	−1.9660
8	0.4400144	−4.36	−0.6194	−0.15581	−0.00540	0.01432	0.01400	−7.043	−0.00070
10	0.4399863	−1.86	−0.1679	−0.02300	0.00278	0.00450	0.00316	−2.059	0.01985
12	0.4399809	−0.916	−0.0569	−0.00427	0.00125	0.00127	0.00075	−0.7205	0.00832
15	0.4399795	−0.381	−0.0150	−0.00045	0.00027	0.00020	0.00012	−0.1934	0.00178
20	0.4399793	−0.122	−0.0027	−0.000017	0.000027	0.000010	0.000003	−0.0346	0.00016

unless something is done to ensure its conservation, the basic properties of the calculated wave can change markedly over a very long time. Reducing ε in order to compensate for this is a relatively inefficient (and ultimately unreliable) way of overcoming the problem.

The conservation of mean surface level and energy can be ensured simply by making a small readjustment at each time-step to the calculated values of Y and Φ. Thus if $\bar{Y}'$ is the mean level after time-stepping, while the true mean level should be $\bar{Y}$, then the true level can be restored simply by subtracting $\bar{Y}' - \bar{Y}$ from each value of Y on the surface. The kinetic and potential energies are obtained using the formulae,

$$KE = \frac{\rho}{2}\int_0^{2\pi} \phi\phi_n \, dx \quad \text{and} \quad PE = \frac{\rho g}{2}\int_0^{2\pi} (Y - \bar{Y})^2 \, dx. \tag{B.1}$$

If the calculated energy is $E' = KE' + PE'$ while the true value should be E then the energy level can (very nearly) be restored by multiplying each value of $Y - \bar{Y}$ and Φ by $\sqrt{E/E'}$. It is clear that such changes always fall within the range of the errors that result both from truncating the Taylor series, used in the time-stepping approximation, and from numerically estimating the time derivatives of the surface motion.

APPENDIX C: SOME HIGH-ORDER NUMERICAL FORMULAE

C.1. Polynomial Fitting at Arbitrary Points; Backward Differencing

Lagrange interpolation [22] can be used to evaluate the coefficients of a polynomial of order n, $f_{(n)}(\zeta)$, that is "fitted" exactly at a set of $n+1$ values such that

$$f_{(n)}(0) = f_0, \quad f_{(n)}(a) = f_a, \quad f_{(n)}(b) = f_b, \quad f_{(n)}(c) = f_c, \tag{C.1}$$

etc. For example, with only six points, such a polynomial can be written explicitly as

$$f_{(5)} - f_0 = \frac{\zeta(\zeta-b)(\zeta-c)(\zeta-d)(\zeta-e)}{a(a-b)(a-c)(a-d)(a-e)}(f_a - f_0) + \cdots + \frac{\zeta(\zeta-a)(\zeta-b)(\zeta-c)(\zeta-d)}{e(e-a)(e-b)(e-c)(e-d)}(f_e - f_0), \tag{C.2}$$

in which successive terms take corresponding forms with the letters $a, \ldots, e$ suitably transposed. Coefficients of different powers of ζ are then easily obtained once the expansions of each of the terms containing $(f_\alpha - f_0)$, for $\alpha \in \{a, \ldots, e\}$, are known. For instance by expanding the term containing $(f_e - f_0)$, one finds

$$\zeta(\zeta-a)(\zeta-b)(\zeta-c)(\zeta-d) = (\zeta, \zeta^2, \zeta^3, \zeta^4, \zeta^5)\begin{pmatrix} abcd \\ -abc-abd-acd-bcd \\ ab+ac+ad+bc+bd+cd \\ -a-b-c-d \\ 1 \end{pmatrix}, \tag{C.3}$$

in which successive coefficients, starting with the last, respectively consist of all possible zeroth order, linear, quadratic, cubic, etc., combinations of the elements of the set $\{-a, \ldots, -d\}$. Corresponding contributions from any other fitted value f_α are obtained by simply transposing letters.

For backward differencing, it remains only to identify the parameters a, b, etc., as times (relative to the current time) at which appropriate derivative values f_a, f_b, etc., are known.

C.2. Fitting to 11 Unit-Spaced Points

This approach can also be applied to polynomial fits at evenly spaced points. Without loss of generality, the spacing between successive points can be considered to be exactly unity so that $f_{(n)}(\zeta)$ is fitted at integral values of ζ.

Supposing now that the function $f = f(\xi)$ is known only at integer values of the parametric variable ξ, then a polynomial approximation of order n for f can be written as follows:

$$f(\xi+\zeta) \approx f_{(n)}(\zeta) = f_0 + a_1\zeta + a_2\zeta^2 + \cdots + a_n\zeta^n, \quad \text{(C.4)}$$

where $f_0 = f(\xi)$. With f_v representing the value of $f(\xi+\zeta)$ at $\zeta = v$, the values of the coefficients a_1, a_2, etc., in a tenth-order centrally fitted polynomial, which is exactly correct at the eleven integer values $-5 \leqslant \zeta \leqslant 5$, are provided by the matrices

$$\begin{pmatrix} 2520\,a_1 \\ 181440\,a_3 \\ 34560\,a_5 \\ 120960\,a_7 \\ 725760\,a_9 \end{pmatrix} = \begin{pmatrix} 2100 & -600 & 150 & -25 & 2 \\ -70098 & 52428 & -14607 & 2522 & -205 \\ 1938 & -1872 & 783 & -152 & 13 \\ -378 & 408 & -207 & 52 & -5 \\ 42 & -48 & 27 & -8 & 1 \end{pmatrix} \times \begin{pmatrix} f_1 - f_{-1} \\ f_2 - f_{-2} \\ f_3 - f_{-3} \\ f_4 - f_{-4} \\ f_5 - f_{-5} \end{pmatrix} \quad \text{(C.5)}$$

and

$$\begin{pmatrix} 50400\,a_2 \\ 362880\,a_4 \\ 172800\,a_6 \\ 120960\,a_8 \\ 3628800\,a_{10} \end{pmatrix} = \begin{pmatrix} -73766 & 42000 & -6000 & 1000 & -125 & 8 \\ 192654 & -140196 & 52428 & -9738 & 1261 & -82 \\ -12276 & 9690 & -4680 & 1305 & -190 & 13 \\ 462 & -378 & 204 & -69 & 13 & -1 \\ -252 & 210 & -120 & 45 & -10 & 1 \end{pmatrix} \times \begin{pmatrix} f_0 \\ f_1 + f_{-1} \\ f_2 + f_{-2} \\ f_3 + f_{-3} \\ f_4 + f_{-4} \\ f_5 + f_{-5} \end{pmatrix}. \quad \text{(C.6)}$$

Clearly, analogous formulae exist for all other orders of polynomial fitting but this 10th-order polynomial suffices for the present discussion. The error in the polynomial approximation (C.4) can be estimated asymptotically as

$$f(\xi+\zeta) - f_{(n)}(\zeta) \sim \frac{f^{[n]}(\xi) + \zeta f^{[n+1]}(\xi)}{(2[n/2]+1)!}\zeta(1-\zeta^2)(2^2-\zeta^2)\cdots([n/2]^2-\zeta^2), \quad \text{(C.7)}$$

where $f^{[k]}(\xi)$ represents the kth derivative of $f(\xi)$ with respect to ξ.

C.3. Formulae for Differentiation; Accuracy

It is clear from this that tenth-order (11-point) estimates of the first and second derivatives of f with respect to ξ at any point are

$$f'(\xi) \approx f'_{(10)}(0) = a_1$$

and

$$f''(\xi) \approx f''_{(10)}(0) = 2a_2. \quad \text{(C.8)}$$

These formulae will only provide accurate estimates of the derivatives if the truncated expansion (C.4) can be considered to be accurate. This requires that any terms of higher power in ζ can realistically be neglected. If f is an *order one function* of a (perhaps spatial) variable $z = h\xi$, then this will only be true, in general, if the data points are "smoothly" distributed and if h is small. This being so, the error term in Eq. (C.7) can be estimated as

$$f(\xi+\zeta) - f_{(10)}(\zeta) \sim \frac{h^{11}}{11!}\left(\frac{d^{11}f}{dz^{11}} + \zeta h\frac{d^{12}f}{dz^{12}}\right) \times \zeta(1-\zeta^2)(2^2-\zeta^2)\cdots(5^2-\zeta^2). \quad \text{(C.9)}$$

Since $f'(\xi)$ and $f''(\xi)$ would be of order h and h^2, respectively, it follows that the relative errors in the formulae (C.8) must be of the order of $(5!)^2 h^{10}/11!$ in both cases. In a similar way, analogous first and second derivative formulae involving polynomials fitted to $M = 2m + 1$ points would involve relative errors of the order of $(m!)^2 h^{M-1}/M! \approx 2^{-M}\sqrt{\pi/m}\,h^{M-1} = O((h/2)^{M-1})$. If the derivatives $d^{11}f/dz^{11}$ and $d^{12}f/dz^{12}$ are indeed comparable in value to unity (that is, not being closer in value to 2^M) the factor of 2^{1-M} in this error-estimate does indeed make a practical difference since M is quite large.

A useful test of the accuracy of the formulae (C.8) is to compare calculated and exact values of derivatives

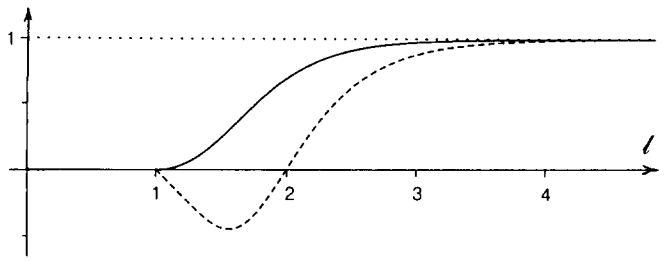

FIG. 12. First (dashed line) and second (solid line) derivatives of sinusoidal and cosinusoidal data, respectively, calculated using 11-point formulae.

of the sinusoidal functions $(l/2\pi)\sin(2\pi\xi/l)$ and $-(l/2\pi)^2\cos(2\pi\xi/l)$. These are periodic over l points and have first and second derivatives of unity (respectively) with respect to ξ at $\xi = 0$. The results of applying the formulae (C.9) are shown in Fig. 12. The second derivative formula is in error by about 30% for a wavelength of only 2 points and rapidly improves to about $2\frac{1}{2}$% at a wavelength of 3 points and $\frac{1}{4}$% for 4 points. The first derivative formula has more difficulty with the shorter wavelengths, mainly because the sine wave of 2-point periodicity cannot be represented at integer values of ξ. The formula recovers quickly however, giving an error of about 12% for a wavelength of 3 points and $1\frac{1}{2}$% for 4 points.

This behaviour is largely responsible for the shape of the numerical dispersion relation shown in Fig. 6. It would clearly improve this calculation if higher-order derivative estimates, or spectral techniques, were to be used [5]. This clearly is a possible option and remains to be investigated further. The present implementation, however, is useful in pointing out both the value and the limitations of using high-order polynomial estimates.

C.4. Smoothing Formulae

C.4.1. *Sawtooth Modes*

We now suppose that the data values at $M = 2m + 1$ consecutive points, $-m \leqslant \zeta \leqslant m$, consist of a polynomial of order $M-2$ and a displacement δ_M which is positive for even points and negative for odd points, representing a sawtooth disturbance. That is,

$$f(\xi+\zeta) \approx f_{(M-2)}(\zeta) + \begin{cases} \delta_M : \zeta \text{ even} \\ -\delta_M : \zeta \text{ odd.} \end{cases} \qquad \text{(C.10)}$$

Fitting this approximation to the points f_ν, leads to the following solutions for δ_M

$$\begin{pmatrix} 2^2\delta_3 \\ 2^4\delta_5 \\ 2^6\delta_7 \\ 2^8\delta_9 \\ 2^{10}\delta_{11} \\ 2^{12}\delta_{13} \\ 2^{14}\delta_{15} \end{pmatrix} = \begin{pmatrix} 2 & -1 & & & & & & \\ 6 & -4 & 1 & & & & & \\ 20 & -15 & 6 & -1 & & & & \\ 70 & -56 & 28 & -8 & 1 & & & \\ 252 & -210 & 120 & -45 & 10 & -1 & & \\ 924 & -792 & 495 & -220 & 66 & -12 & 1 & \\ 3432 & -3003 & 2002 & -1001 & 364 & -91 & 14 & -1 \end{pmatrix} \times \begin{pmatrix} f_0 \\ f_1+f_{-1} \\ f_2+f_{-2} \\ f_3+f_{-3} \\ f_4+f_{-4} \\ f_5+f_{-5} \\ f_6+f_{-6} \\ f_7+f_{-7} \end{pmatrix} \qquad \text{(C.11)}$$

for all values of M between 3 and 15. An M-point sawtooth smoothing of a function f would be achieved by subtracting the values of $\delta_M(\xi)$ from the values of $f(\xi)$ at each value of ξ. It is worth noting that the formula for δ_{11} is identical to the formula for the last term in the polynomial fitted to 11 points—a_{10} in (C.6) above—apart from a constant factor. This is not a coincidence and an analogous relationship is found for each of the formulae for δ_M for any odd positive integer value of M.

This reveals another significant interpretation of the rôle of these formulae. Recalling that the coefficients in the polynomial approximation (C.4) should decrease towards negligible values if truncation of the series to a finite polynomial is to provide a good approximation, it is clear that the last terms in each of these polynomials should also be very small. Being a measure of the magnitude of these last terms, the smoothing formulae (C.11) should thus provide some measure of the accuracy of the polynomial approximation to any given set of points.

Alternatively, applying a smoothing formula to the function $f(\xi)$—subtracting the values of $\delta_M(\xi)$ for an appropriate value of M—may be thought of as an attempt to reduce the values of the final coefficients in the polynomial approximation in order to recover some semblance of

accuracy after (say) some numerical instability or simply a lack of resolution has caused them to increase unacceptably.

C.4.2. *Sawtooth Modes and Modes with 3-Point Periodicity*

More severe smoothing of the data can be achieved by also removing modes that are periodic over more than two points. It was seen in Section 7.3 that disturbances periodic over three points may be expected to follow the two-point or sawtooth modes in becoming unstable. The formula (C.10) can be extended to include all three-point periodic modes with zero mean value as follows,

$$f(\xi+\zeta) \approx f_{(M-4)}(\zeta) + \left\{ \begin{matrix} \delta_M^{(2)} : \zeta \text{ even} \\ -\delta_M^{(2)} : \zeta \text{ odd} \end{matrix} \right\} + \left\{ \begin{matrix} 2\delta_M^{(3)} : \zeta = 3l \\ -\delta_M^{(3)} \ : \zeta = 3l \pm 1 \end{matrix} \right\} + \left\{ \begin{matrix} 0 \ : \zeta = 3l \\ \pm\tilde{\delta}_M^{(3)} : \zeta = 3l \pm 1 \end{matrix} \right\} \tag{C.12}$$

in which l represents any integer.

Matrices that are associated with solving for $\delta_M^{(2)}$, $\delta_M^{(3)}$, and $\tilde{\delta}_M^{(3)}$, as well as the polynomial coefficients in terms of function values at evenly spaced points centrally located about $\zeta = 0$, are only non-singular for $M = 3$, 9, 15, etc. In two of these cases, solving for $\delta_M^{(2)}$ and $\delta_M^{(3)}$ gives

$$\begin{pmatrix} 64\,\delta_9^{(2)} \\ 54\,\delta_9^{(3)} \\ 4096\,\delta_{15}^{(2)} \\ 1458\,\delta_{15}^{(3)} \end{pmatrix} = \begin{pmatrix} 10 & -11 & 10 & -5 & 1 & & & \\ 10 & -4 & -4 & 4 & -1 & & & \\ 660 & -627 & 517 & -341 & 166 & -55 & 11 & -1 \\ 264 & -165 & -22 & 121 & -100 & 43 & -10 & 1 \end{pmatrix} \times \begin{pmatrix} f_0 \\ f_1+f_{-1} \\ f_2+f_{-2} \\ f_3+f_{-3} \\ f_4+f_{-4} \\ f_5+f_{-5} \\ f_6+f_{-6} \\ f_7+f_{-7} \end{pmatrix}. \tag{C.13}$$

Smoothing is achieved by subtracting $\delta_M^{(2)}(\xi)$ and $2\delta_M^{(3)}(\xi)$ from $f(\xi)$ at each value of ξ. In the cases $M = 9$ and $M = 15$ this is equivalent to subtracting $\tilde{\delta}_M(\xi) = \delta_M^{(2)} + 2\delta_M^{(3)}$, where

$$\begin{pmatrix} 1728\,\tilde{\delta}_9 \\ 2985984\,\tilde{\delta}_{15} \end{pmatrix} = \begin{pmatrix} 910 & 1562484 \\ -553 & -1132923 \\ 14 & 286781 \\ 121 & 247027 \\ -37 & -288586 \\ & 136033 \\ & -32941 \\ & 3367 \end{pmatrix}^{\mathrm{T}} \begin{pmatrix} f_0 \\ f_1+f_{-1} \\ f_2+f_{-2} \\ f_3+f_{-3} \\ f_4+f_{-4} \\ f_5+f_{-5} \\ f_6+f_{-6} \\ f_7+f_{-7} \end{pmatrix} \tag{C.14}$$

ACKNOWLEDGMENTS

This work was supported by the Science and Engineering Research Council. The author is also grateful to Professor D. H. Peregrine and to Drs. M. Mizuguchi and M. Tanaka for their helpful advice during many useful and interesting discussions.

REFERENCES

1. I. A. Svendsen, "Mixed Boundary Value Problem for Laplace's Equation in Domain of Arbitrary Shape," Coastal Engineering Laboratory Report, Technical University of Denmark, 1971 (unpublished).
2. M. S. Longuet-Higgins and E. D. Cokelet, *Proc. R. Soc. London A* **350**, 1 (1976).
3. T. Vinje and P. Brevig, *Adv. Water Resour.* **4**, 77 (1981).
4. G. R. Baker, D. I. Meiron, and S. A. Orszag, *J. Fluid Mech.* **123**, 477 (1982).
5. A. J. Roberts, *IMA J. Appl. Math.* **31**, 13 (1983).
6. B. Fornberg, *SIAM J. Sci. Stat. Comput.* **1**, 386 (1980).
7. S. Grilli, J. Skourup and I. A. Svendsen, *Eng. Anal. Boundary Elements* **6**, 97 (1989).
8. D. W. Moore, *IMA J. Appl. Math.* **31**, 1 (1983).
9. J. W. Dold and D. H. Peregrine, in *Proceedings of 19th Intnl. Conf. on Coastal Engineering, Houston 1984*, p. 955.
10. J. W. Dold and D. H. Peregrine, in *Numerical Methods for Fluid Dynamics II*, edited by K. W. Morton and M. J. Baines (Clarendon Press, Oxford, 1985).
11. M. Tanaka, J. W. Dold, M. Lewy, and D. H. Peregrine, *J. Fluid Mech.* **185**, 235 (1987).
12. J. W. Dold and D. H. Peregrine, in *Proceedings of 20th Intnl. Conf. on Coastal Engineering, Taipei 1986*, Vol. 1, p. 163.
13. M. J. Cooker, Ph. D. Thesis, University of Bristol, 1989 (unpublished).
14. M. J. Cooker, D. H. Peregrine, C. Vidal, and J. W. Dold, *J. Fluid Mech.* **215**, 1 (1990).
15. A. F. Teles da Silva, Ph. D. Thesis, University of Bristol, 1989 (unpublished).
16. P. McIver and D. H. Peregrine, "Motion of a Free Surface and Its Representation by Singularities," Bristol University Report, 1981 (unpublished).
17. J. Rohklin, *Comput. Phys.* **60**, 187 (1985).
18. J. Reichel, *J. Sci. Stat. Comput.* **11**, 263 (1990).
19. M. Tanaka, *J. Phys. Soc. Jpn.* **52**, 3047 (1983).
20. M. S. Longuet-Higgins, *Proc. R. Soc. London A* **360**, 471 (1978).
21. A. F. Teles da Silva and D. H. Peregrine, *J. Fluid Mech.* **195**, 218 (1988).
22. R. L. Burden and J. D. Faires, *Numerical Analysis* (PWS-KENT, Boston, 1989), p. 91.